The Astrophysical Journal, 622:629–652, 2005 March 20

A FAR-ULTRAVIOLET SPECTROSCOPIC SURVEY OF LUMINOUS COOL STARS

A. K. Dupree, A. Lobel, and P. R. Young[1]
Harvard-Smithsonian Center for Astrophysics, 60 Garden Street, Cambridge, MA 02138; adupree@cfa.harvard.edu, alobel@cfa.harvard.edu, p.r.young@rl.ac.uk

T. B. Ake
Johns Hopkins University/CSC, Charles and 34th Street, Baltimore, MD 21218; ake@pha.jhu.edu

and

J. L. Linsky and S. Redfield[2]
JILA, University of Colorado and NIST, Boulder, CO 80309-0440; jlinsky@jila.colorado.edu, sredfiel@astro.as.utexas.edu
Received 2004 August 26; accepted 2004 December 13

ABSTRACT

The *Far Ultraviolet Spectroscopic Explorer* (*FUSE*) ultraviolet spectra of eight giant and supergiant stars reveal that high-temperature (3×10^5 K) atmospheres are common in luminous cool stars and extend across the color-magnitude diagram from α Car (F0 II) to the cool giant α Tau (K5 III). Emission present in these spectra includes chromospheric H Lyβ, Fe II, C I, and transition region lines of C III, O VI, Si III, and Si IV. Emission lines of Fe XVIII and Fe XIX signaling temperatures of $\sim 10^7$ K and coronal material are found in the most active stars, β Cet and 31 Com. A short-term flux variation, perhaps a flare, was detected in β Cet during our observation. Stellar surface fluxes of the emission of C III and O VI are correlated and decrease rapidly toward the cooler stars, reminiscent of the decay of magnetically heated atmospheres. Profiles of the C III λ977 lines suggest that mass outflow is underway at $T \sim 80,000$ K and the winds are warm. Indications of outflow at higher temperatures (3×10^5 K) are revealed by O VI asymmetries and the line widths themselves. High-temperature species are absent in the M supergiant α Ori. Narrow fluorescent lines of Fe II appear in the spectra of many giants and supergiants, apparently pumped by H Lyα, and formed in extended atmospheres. Instrumental characteristics that affect cool star spectra are discussed.

Subject headings: stars: chromospheres — stars: winds, outflows — ultraviolet: stars

1. INTRODUCTION

The structure of the outer atmospheres of cool giant and supergiant stars can reveal the evolution of magnetic activity as atmospheres expand, stars lose angular momentum, and arguably dynamo heating decreases, as stars become cooler and more luminous. The existence of hot material and its relation to winds and mass loss can be addressed with far-ultraviolet spectra obtained with the *Far Ultraviolet Spectroscopic Explorer* (*FUSE*) satellite (Moos et al. 2000) because they probe both the presence of high-temperature plasma and the dynamics of the atmosphere. Two well-recognized examples of these extremes are represented by the Sun (possessing a hot, fast, low-mass flux wind) and the supergiant α Ori (possessing a cool, slow, high-mass flux wind). However, identifying the connecting links between these two types of atmospheres, perhaps represented in part by the hybrid stars (Hartmann et al. 1980; Reimers et al. 1996), can be addressed by *FUSE* spectra. Thus, far-ultraviolet spectra can be used to build a comprehensive picture of the heating and dynamics of the outer atmospheres of cool stars.

Ultraviolet measurements with the *International Ultraviolet Explorer* (*IUE*) laid the foundations for characterization of cool star atmospheres (see Jordan & Linsky 1989; Dupree & Reimers 1989); the *Hubble Space Telescope* (*HST*) has focused principally on individual objects (e.g., Ayres et al. 1998; McMurry & Jordan 2000; Carpenter et al. 1999; Robinson et al. 1998; Lobel & Dupree 2001). *FUSE* complements *IUE* and *HST* because coverage of shorter wavelengths (912–1180 Å) gives access to the strong O VI resonance emission formed at temperatures $\sim 3 \times 10^5$ K, providing a diagnostic of temperatures higher than normally available in the near-ultraviolet, and line profiles provide clues to heating and atmospheric dynamics. This spectral region also contains fine-structure transitions of Fe XVIII and Fe XIX that enable detection of a hot corona and its dynamics and extend the temperature coverage by more than an order of magnitude to 7×10^6 K in addition to allowing velocity and profile measurements. A summary of the major atomic transitions specifically considered here is contained in Table 1.

Eight luminous stars, β Cet (HD 4128), α Ori (HD 39801), α Tau (HD 29139), α Car (HD 45348), β Gem (HD 62509), 31 Com (HD 111812), β Dra (HD 159181), and α Aqr (HD 209750), were selected by the Cool Stars team on the *FUSE* satellite in order to obtain far-UV spectra of objects of various effective temperatures, degrees of activity, and luminosities (see Fig. 1). Parameters of these stars are given in Table 2. Analysis of these spectra is presented here. A complementary paper on the survey of cool dwarf stars with *FUSE* is reported by Redfield et al. (2002).

2. OBSERVATIONS AND DATA REDUCTION

The *FUSE* instrument and its calibration are discussed in Moos et al. (2000) and Sahnow et al. (2000). *FUSE* has four co-aligned prime focus telescopes that feed light to four Rowland spectrographs. Two of the spectrograph gratings are coated with LiF and two with SiC (Moos et al. 2000), enabling full (and redundant, in some regions) coverage of the *FUSE* wavelength

[1] Current address: Rutherford Appleton Laboratory, Space Science and Technology, Department Chilton, Didcot, Oxford OX11 0QX, UK.
[2] Current address: McDonald Observatory, University of Texas, 1 University Station, Austin, TX 78712-1083.

TABLE 1

Major Atomic Transitions Considered Here

Ion	Transition[a]	Wavelength (Å)	$T_{\rm formation}$[b] (K)
Fe II	Many[c]	1106–1143	1.8×10^4
C III	$2s^22p\ ^1S_0$–$2s2p^2\ ^1P_1$	977.02	8.3×10^4
	$2s2p\ ^3P_{0,1,2}$–$2p^2\ ^3P_{0,1,2}$	1176[d]	8.3×10^4
O VI	$2s\ ^2S_{1/2}$–$2p\ ^2P_{3/2}$	1031.92	2.9×10^5
	$2s\ ^2S_{1/2}$–$2p\ ^2P_{1/2}$	1037.61	2.9×10^5
Fe XVIII	$2p^5\ ^2P_{3/2}$–$2p^5\ ^2P_{1/2}$	974.86	6.6×10^6
Fe XIX	$2p^4\ ^3P_2$–$2p^4\ ^3P_1$	1118.07	7.9×10^6

[a] Atomic configuration expressed as lower level (i) to upper level (j) where emission corresponds to the transition $j \rightarrow i$.

[b] Temperatures correspond to the temperature of peak emission rate in a collisionally dominated plasma and were calculated with version 4 of the CHIANTI database (Young et al. 2003) using the ionization balance calculations of Mazzotta et al. (1998) and an electron density of 10^{10} cm^{-3}.

[c] Fe II emission in these stars results from fluorescent and cascade processes involving many configurations, and the temperature of "formation" does not strictly apply since the population of levels is not linked to the local electron temperature.

[d] There are six components to this multiplet.

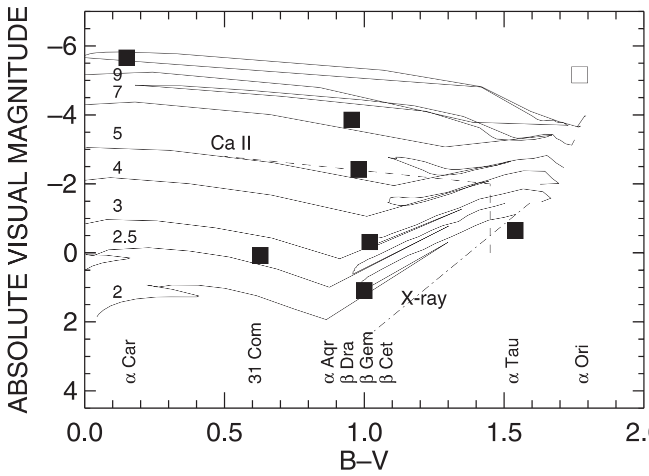

Fig. 1.—Target stars included in the *FUSE* luminous star survey. Evolutionary tracks are shown for stars of solar mass 2–9 (Schaller et al. 1992); the locus marking the "disappearance" of X-rays in giant stars (Hünsch & Schröder 1996) is indicated (*dot-dashed line*, labeled "X-ray"). Stars in the region above and to the right of the dashed line (labeled "Ca II") exhibit narrow circumstellar absorption components believed to be associated with a wind (Reimers 1977). Filled squares mark the stars having C III and O VI emission; α Ori (*open square*) displays neither C III nor O VI emission.

range: 905–1179 Å. The spectral segments are denoted by the grating coating and telescope (e.g., LiF1, LiF2 and SiC1, SiC2) and by the detector (A or B). The monochromatic spectral resolving power of *FUSE* is 20,000 ± 2000 (*FUSE* Observer's Guide, version 4.0[3]) or ~15 km s^{-1}. With good signal-to-noise ratio in a line profile and the oversampling of the *FUSE* spectrum, the position of a spectral line can be determined to about 2 km s^{-1}.

All spectra were obtained through the large aperture of *FUSE* (denoted LWRS, a 30″ square); α Tau was also observed through the 4″ × 20″ square medium aperture (MDRS) in order to minimize airglow contamination. Details of the *FUSE* observations are noted in Table 3. Spectra were reduced with the *FUSE* CalFUSE version 2.0.5 pipeline, except CalFUSE version 2.4 was used for α Tau in the LWRS aperture. To combine exposures, individual subexposures for a single telescope/detector combination (i.e., LiF1A, SiC2A, etc.) were co-added after alignment using cross-correlation techniques. Restricted wavelength ranges for the cross-correlation were chosen for each detector segment so as to avoid geocoronal emission and to perform the cross-correlation alignment on strong stellar features. Extractions of spectra obtained only during nighttime pointings were made for all targets in addition to the normal procedures of extracting "both" spectra (both day and night combined).

Individual images were examined to ensure that exposures with burst characteristics were not included and the star was in the aperture in all channels. However, it is difficult to identify placement in the MDRS aperture where the star may be close to the edge of the aperture (see also Redfield et al. 2002). Data from the large-aperture LWRS are used for flux measurements of all targets. Special attention was given to the SiC channels to verify that the target was in the aperture. The spacecraft guiding is maintained using the LiF1A channel, and the SiC channels can become misaligned. In several subexposures of α Tau and β Dra, the C III λ977 emission was not visible and we eliminated that subexposure from the summations (see Table 3 for a summary).

Another potential contaminant is scattered sunlight that can affect both the fluxes and profiles of the C III λ977 and O VI λ1032 transition. Comparison of day and night extractions can identify the presence of a solar component. Scattered sunlight is present in the α Tau spectrum in the LWRS aperture, where the nighttime extractions were used for the SiC2A and LiF1A channels (see Table 3).

Short-wavelength spectra for the eight targets are shown in Figure 2, and the corresponding long-wavelength spectra are shown in Figure 3.

3. WAVELENGTH SCALE

The relative wavelength scale for each detector segment of each channel is determined by the CalFUSE pipeline and believed to be accurate to 3–4 pixels (~0.025 Å or 8 km s^{-1}) over most of the detectors.[4] However, the absolute velocity offset for each detector must be determined independently in each detector segment. Narrow interstellar absorption lines of C III λ977 and C II λ1036 can be identified in the spectra from the SiC2A and LiF1A channels, respectively, where they occur in the profiles of the stellar emission lines. Ultraviolet spectra from *HST* (STIS/GHRS) typically contain interstellar lines of low-ionization species (C II, Si III, D I, O I, and Mg II) whose velocities are measured; these values are used to set the absolute wavelength scale of the *FUSE* spectra (see Table 4). Two stars, α Aqr and β Dra, show interstellar H_2 near 1038 Å, and interstellar C II λ1036.34 can be identified in α Aqr. However, in the LiF1A channels, four targets (31 Com, β Gem, α Ori, and α Tau) show no discernible interstellar feature and had to be treated differently. For β Gem, several chromospheric lines (C II λ1036.3367 [short-wavelength wing only], C II λ1037.0182, S IV λ1062.621, Si IV λ1066.6094, and S IV λ1072.9558) were fitted to Gaussian curves and assigned a photospheric velocity. The average offset for β Gem was determined to be 0.0351 ± 0.008 Å. The star 31 Com is more difficult because only two weak stellar S IV lines are available ($\lambda\lambda$1062.6166, 1072.9954), which give offsets of −0.0571 and −0.0099 Å, respectively, an

[3] Available at http://fuse.pha.jhu.edu/support/guide/guide_V4.0.html#INRES.

[4] See the *FUSE* Wavelength Calibration: A *FUSE* White Paper at http://fuse.pha.jhu.edu/analysis/calfuse_wp1.html.

TABLE 2
Stellar Parameters

Star	Other Name	Spectral Type	Distance (pc)	V	$V-R$	α[a]	$v_{\rm rad}$[b] (km s^{-1})	References
β Cet	HD 4128	K0 III	29.4	2.02	+0.72	6.74E15	+13.4	1, 2, 3, 4
α Tau	HD 29139	K5 III	20.0	0.86	+1.23	3.09E14	+54.0	1, 2, 3, 5
α Ori	HD 39801	M2 Iab	131	0.42	+1.64	5.31E13	+21.0	1, 2, 3
α Car	HD 45348	F0 II	95.9	−0.75	+0.24	3.50E15	+20.5	1, 2, 3
β Gem	HD 62509	K0 IIIp	10.3	1.15	+0.75	2.69E15	+2.81	1, 2, 3, 5
31 Com	HD 111812	G0 IIIp	94.2	4.94	+0.55	1.94E17	−1.25	1, 2, 3, 5
β Dra	HD 159181	G2 Ib–IIa	110	2.79	+0.68	1.60E16	−21.6	1, 2, 3, 5
α Aqr	HD 209750	G2 Ib	~230	2.95	+0.66	2.01E16	+6.8	1, 3, 4

[a] The factor, α, relates the flux observed at Earth to the stellar surface flux $F_* = \alpha F_\oplus$ and $\alpha = (d/R_*)^2 = 1.7018 \times 10^{17}/\phi^2$ with ϕ(mas) evaluated from the Barnes-Evans relationships (Barnes et al. 1978).
[b] Parameter $v_{\rm rad}$ denotes the heliocentric radial velocity of the star.
References.—(1) Perryman et al. 1997; (2) Wilson 1953; (3) Johnson et al. 1966; (4) Beavers & Eitter 1986; (5) de Medeiros & Mayor 1999.

uncomfortable spread of 13 km s^{-1}. Having no other alternative, we take the average offset (−0.0335 Å) to set the absolute wavelength scale. For α Ori and α Tau, the CalFUSE 2.0.5 wavelength scale is adopted here.

FUSE channels at the longest wavelength (1100–1180 Å) generally do not contain observable interstellar lines in the spectra of cool stars. In this case we resort to *HST* spectra obtained with the Space Telescope Imaging Spectrograph (STIS) or the Goddard High Resolution Spectrograph (GHRS). For the LiF2A (and Lif1B) channel we adopt the *HST* STIS/GHRS absolute wavelength offset by forcing agreement between the *HST* and *FUSE* wavelengths using C III λ1176 when observed in both spectra. Otherwise, we have forced the velocity of the ions observed in LiF2A (Si III λ1113.23 and Si IV λ1122.49) to match the same ion, Si III λ1206 and Si IV $\lambda\lambda$1394, 1401, observed with *HST.*

The velocity offsets necessary for alignment with previously observed interstellar line velocities are usually small. For six targets of this program (not including α Tau and α Ori), the corrections for the C III line (SiC2A channel) ranged in absolute value from 4.4 to 29 km s^{-1} with an average of 11.5 km s^{-1}. The LiF2A channel for the same six targets gave offsets ranging from −0.0335 (−9.7 km s^{-1}) to +0.06873 Å (+17.5 km s^{-1}) with an average of 0.0245 Å (+6.25 km s^{-1}).

Comparison of the wavelength offsets obtained in this way was made with wavelengths of unblended O I airglow lines observed in the spectrum for several cases. Airglow lines typically vary in wavelength by 5–18 km s^{-1} from the offset determined by the interstellar features, so they can give a crude estimate of the absolute scale, but only to roughly ±10 km s^{-1}. For β Gem, the O I airglow gives an offset for SiC2A of +17.5 km s^{-1} as compared to the interstellar offset of +15.0 km s^{-1}. In the LiF2A channel, the airglow values vary from +5 to +18 km s^{-1}, different from the offsets determined by interstellar lines. Although lack of precision in the wavelength scale exists, this does not materially affect the line identifications and fluxes or conclusions drawn from the analysis of line profiles.

4. LINE IDENTIFICATIONS

Line identifications were made by comparison to the solar spectrum (Curdt et al. 2001) and to other cool luminous stars observed by *FUSE* (Young et al. 2001; Ake et al. 2000). The highest ionization lines (Fe XVIII and Fe XIX) are discussed separately below. The strongest species are marked in Figures 2 and 3. Every star, except for α Ori, exhibits emission from C III and O VI, indicating that temperatures at least as high as 3×10^5 K are present assuming a collision-dominated thermal plasma. Emission

TABLE 3
Targets and *FUSE* Observation Log

Star	Other Name	Spectral Type	Data Set	Observation Date	Exposure (ks)	Aperture
β Cet	HD 4128	K0 III	P1180501	2000 Dec 10	13.1	LWRS
α Ori	HD 39801	M2 Iab	P1180901	2000 Nov 3	10.3	LWRS
α Tau	HD 29139	K5 III	P1040901	2001 Jan 14	12.2[a]	MDRS
	...	...	P2180601	2003 Sep 14	6.3	LWRS
	...	...	P2180602	2003 Sep 15	12.2	LWRS
	...	...	P2180603	2003 Sep 15	10.4	LWRS
α Car	HD 45348	F0 II	P1180101	2000 Dec 11	5.6	LWRS
	...	...	P2180101	2001 Oct 25	5.9	LWRS
	...	...	P2180102	2001 Oct 26	10.7	LWRS
β Gem	HD 62509	K0 IIIp	P1180601	2000 Nov 11	21.8	LWRS
31 Com	HD 111812	G0 IIIp	P1180401	2001 Apr 20	12.2	LWRS
β Dra	HD 159181	G2 Ib–IIa	P1180301	2000 May 9	5.6	LWRS
	...	...	P2180301	2001 Jun 30	16.4[b]	LWRS
α Aqr	HD 209750	G2 Ib	P2180201	2001 Jun 16	34.3	LWRS
	...	...	P2180202	2001 Oct 7	10.5	LWRS

[a] The SiC1B channels were on the target for a total of 1790 s and the SiC2A exposure totaled 3182 s.
[b] SiC1B channel: exposure 3 (1635 s) was not on target.

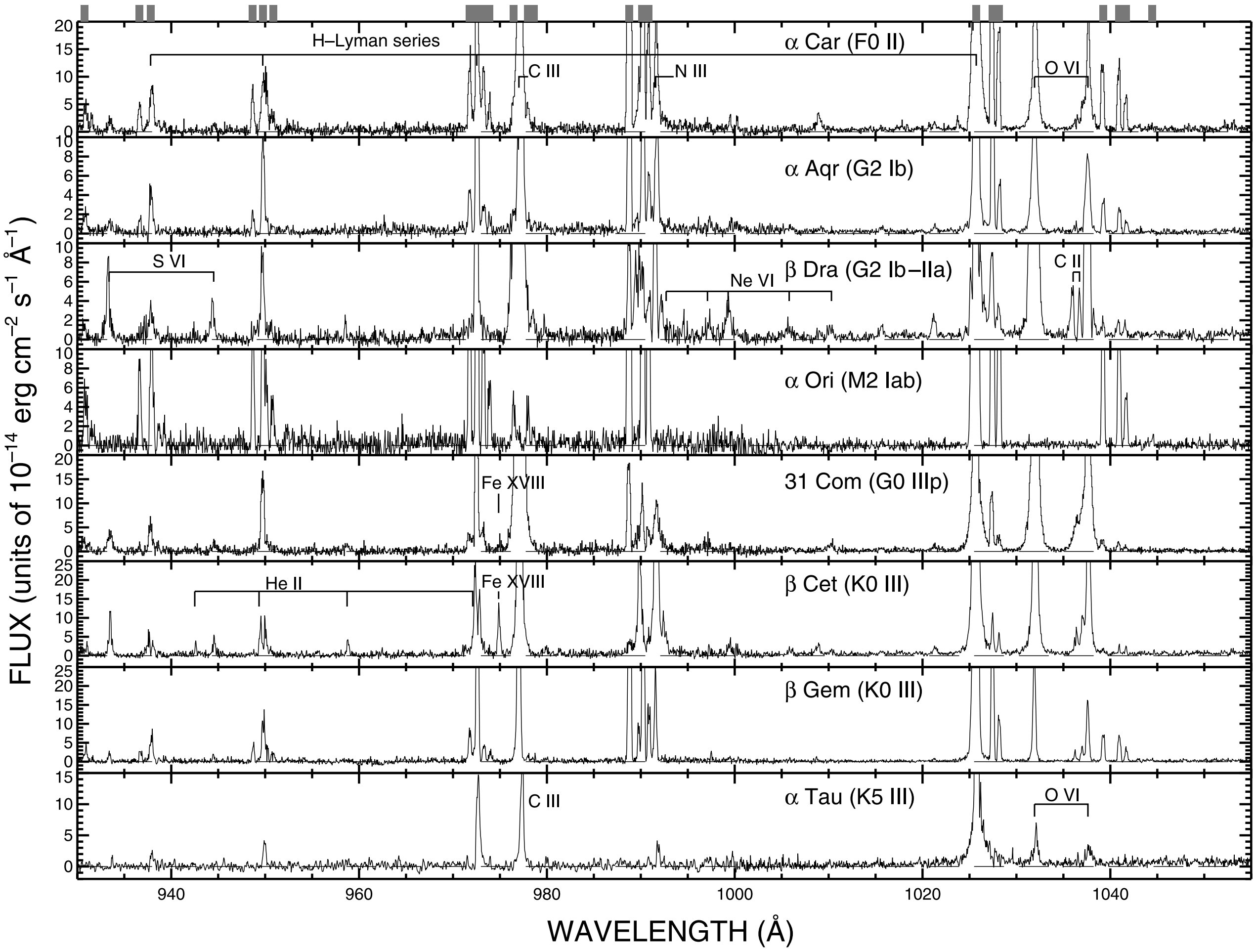

FIG. 2.—*FUSE* spectra of the sample of luminous cool stars in the region 930–1055 Å. Spectra from each detector (SiC2A and LiF1A) have been cross-correlated and summed for all images, then rebinned by a factor of 8 for display. Prominent emission features are identified. Strong airglow lines are frequently truncated, and their positions are noted by the hatched area at the top of the figure.

from the Earth's atmosphere ("airglow") is identified using several spectra with long integrations on the sky.[5]

Fluxes were extracted (Table 5) for the strongest lines of C III ($\lambda\lambda$977 and 1176) and O VI (λ1032) by integrating directly over the line profiles. These fluxes agree with previous *Orbiting and Retrievable Far and Extreme Ultraviolet Spectrometer* (*ORFEUS*) measurements (Dupree & Brickhouse 1998) of α Aqr and β Dra to within 6% on average; an exception is λ1176, which is stronger in the *FUSE* spectrum of α Aqr by a factor of 2.5. Such a large discrepancy is unexpected. Because the *FUSE* spectra for these two stars were taken through the large aperture, they are not subject to flux loss as found in some medium-aperture spectra (Redfield et al. 2002). The supergiant α Aqr exhibits periodic chromospheric variability (Rao et al. 1993) and variability in the Mg II flux (Brown et al. 1996), which may account in part for the discrepancy. Cool dwarf stars studied with *FUSE* (Redfield et al. 2002) also show discrepancies, on average of 20%, when compared to fluxes from *ORFEUS*.

Luminous cool stars show a distinct pattern of narrow emission lines near 1130–1140 Å first noted in the *ORFEUS* spectrum of α TrA and ascribed to low-ionization states most probably fluoresced in the extended cool atmosphere (Dupree & Brickhouse 1998). It required the higher spectral resolution of *FUSE* to identify many of the emission lines as Fe II (Harper et al. 2001) that result from fluorescent decay of levels pumped by Lyα (e.g., Hartman & Johansson 2000). The targets in this survey also show many of the same narrow lines (see Fig. 4).

Details of the Fe II line strengths are puzzling. The cool giant α Tau displays a strong Fe II spectrum, where it appears that Fe II lines pumped by radiation close to the Lyα core (<1.8 Å) are present and strong and lines pumped by more distant wavelengths are absent or weaker as suggested by Harper et al. (2001) based on a spectrum of α TrA. The strong signature transitions of Fe II between 1131 and 1139 Å support this conjecture. However, the Fe II lines do not have similar relative strengths in other targets. Whereas 1131.594 Å dominates in the spectrum of α Tau, α Ori, β Dra, and α Aqr, another transition of Fe II at 1138.941 Å dominates in β Gem and β Cet, appears in α Tau, β Dra, and α Aqr, but is very weak or absent in α Ori. Moreover, the supergiant α Ori has a more extensive atmosphere than the giant α Tau, which would appear to enhance fluorescent processes, yet the fluoresced lines appear weaker in α Ori than in α Tau. Because the presence of the fluoresced lines depends on the intrinsic stellar Lyα profile shape, its flux, and the detailed atmospheric dynamics to enable the process, models specific to each star need to be constructed to interpret these spectra.

It is worth noting that the low background count rate of the *FUSE* detectors enables identification of weak emission features. As shown in Figure 5, longward of the C III λ977 emission, the spectrum of β Dra exhibits, not airglow, but an O I line

[5] We extracted a sky exposure of ~58 ks from the LWRS from observation P1100301; another airglow spectrum can be found on the *FUSE* Web site, http://fuse.pha.jhu.edu/analysis/airglow/airglow.html.

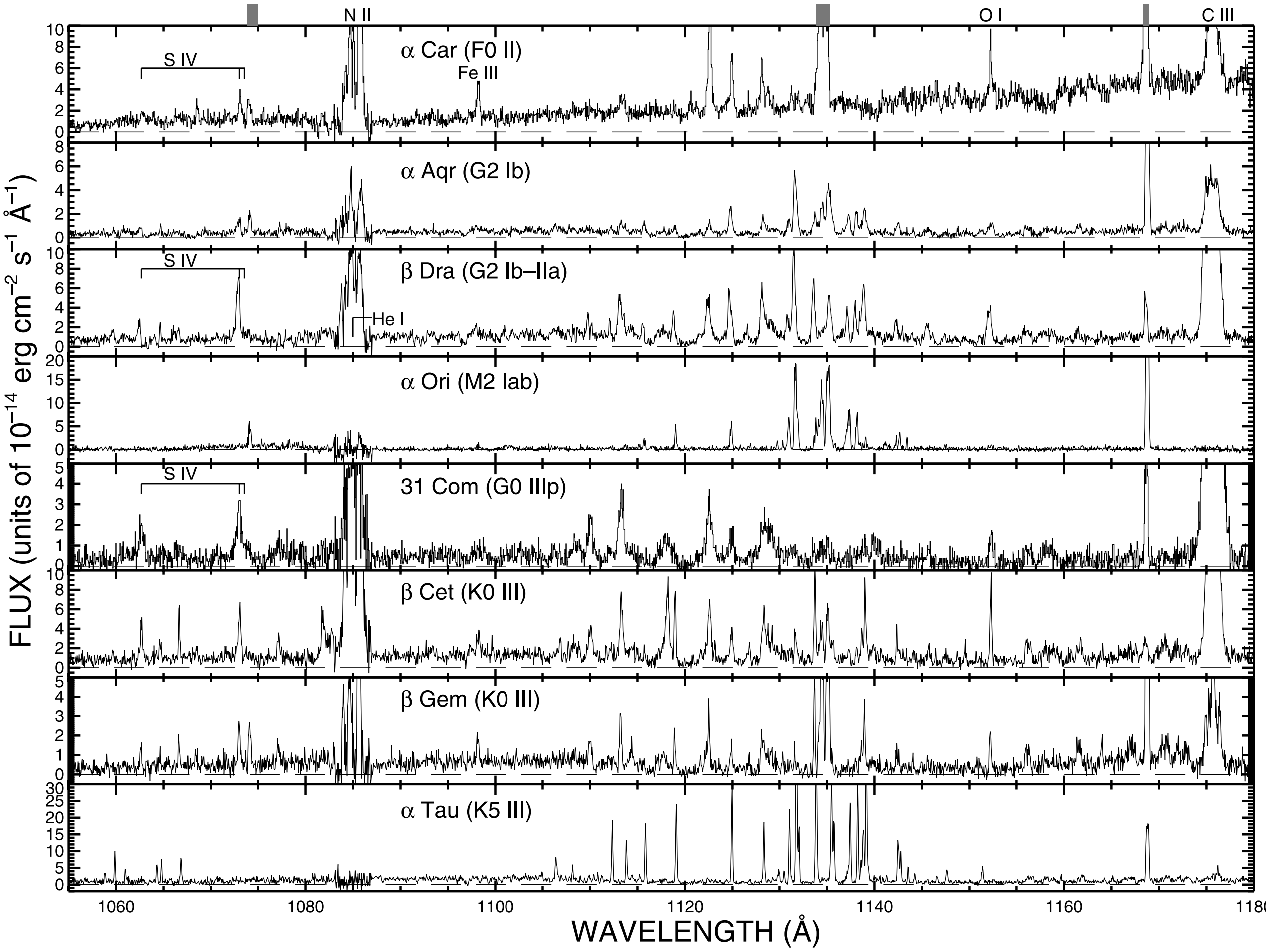

FIG. 3.—*FUSE* spectra of the sample of the cool star survey in the range 1055–1180 Å. Detailed identifications of the complex region between 1110 and 1145 Å are given in Fig. 4. Shaded regions at the top of the figure indicate positions of potential contamination by geocoronal emission.

TABLE 4

Interstellar Medium Lines: Heliocentric Velocities

Star	Other Name	Species	λ (Å)	$V_{\rm ISM}$ (km s^{-1})	Note
β Cet	HD 4128	C II	1334	+5.8	1
	...	Si III	1206	+4.5	1
	...	D I	1215	+4.7	1
	...	O I	1302	+6.6	1
		Average adopted	...	+5.4	
α Tau	HD 29139	Mg II	2795	−30.	2
	...	O I	1302	−30.	2
α Ori	HD 39801	Not available			
α Car	HD 45348	H Lyα	1215.	+25.	3
β Gem	HD 62509	Mg II (averaged)	2800	+26.1	4
31 Com	HD 111812	Mg II	2800	−3.4	5
	...	Fe II	2599	−2.4	5
	...	D I	1216	−2.7	5
	...	C II	1335	−3.8	6
	...	O I	1302	−2.6	6
		Average adopted	...	−3.2	
β Dra	HD 159181	Mg II	2800	−20.	7
α Aqr	HD 209750	Mg II	2800	−18	8

NOTES.—(1) Measured from STIS spectrum. (2) Robinson et al. 1998. (3) Marilli et al. 1997. (4) Dring et al. (1997) find two interstellar components at +22.0 ± 1.8 and +33.2 ± 1.8 km s^{-1}, of which the 22 km s^{-1} cloud has a larger column density by a factor of 1.7; an average value, weighted by the column density, is used, viz., $(N_1/N_{\rm tot})V_1 + (N_2/N_{\rm tot})V_2 = V_{\rm avg}$. (5) Values taken from Dring et al. (1997); in agreement with independent determination by Piskunov et al. (1997). (6) Redfield & Linsky (2004). (7) Measured from GHRS spectra calibrated with Pt Lamp. (8) *IUE* spectra from Drake et al. (1984).

TABLE 5
EMISSION-LINE FLUXES

STAR	C III λ977[a] Flux (ergs cm^{-2} s^{-1})	C III λ977[a] Counts	C III λ1176[b] Flux (ergs cm^{-2} s^{-1})	C III λ1176[b] Counts	O VI λ1032[c] Flux (ergs cm^{-2} s^{-1})	O VI λ1032[c] Counts
β Cet	6.55E−13	4503	3.12E−13	4686	5.86E−13	10044
α Tau	7.00E−14	284	4.91E−14	518	3.34E−14	372
α Car	3.40E−13	4220	1.30E−13	6288	2.16E−13	6949
β Gem	2.90E−13	3357	6.95E−14	1780	1.07E−13	3177
31 Com	1.01E−12	7141	5.65E−13	8400	5.09E−13	8959
β Dra	1.52E−12	18203	4.54E−13	11694	8.03E−13	24133
α Aqr	2.77E−13	6226	7.75E−14	4233	1.04E−13	6188

NOTES.—Total flux observed at Earth in the emission line obtained by integration over the line profile. Errors in the flux can be taken as ±10% corresponding to the uncertainty in the *FUSE* absolute calibration.
[a] Measured from SiC2A channel.
[b] Measured from LiF2A channel.
[c] Measured from LiF1A channel. A small background continuum was subtracted from the flux values, although the counts include the total of line plus continuum.

at 977.62 Å that is fluoresced most probably by the C III transition itself through the stellar resonance O I transition at 976.45 Å with the same upper level ($5s\ ^3S_1$), overlapping the broad C III profile.

5. CORONAL LINES

Two targets, β Cet and 31 Com, contain emission from high-temperature coronal species: Fe XVIII and Fe XIX. This is not surprising since these very same ions have been identified in *Extreme Ultraviolet Explorer* (*EUVE*) spectra of these stars (Sanz-Forcada et al. 2002). Similar transitions were found in the *FUSE* spectrum of Capella (Young et al. 2001) and other targets discussed by Redfield et al. (2003), including β Cet and 31 Com. Coronal species are present in the near-ultraviolet region covered by *HST*; these include Fe XII and Fe XXI (Jordan et al. 2001; Ayres et al. 2003).

5.1. *β Cet*

Star β Cet shows the highest excitation lines in the *FUSE* spectral region, namely, Fe XVIII λ974.86 ($2s^22p^5\ ^2P_{3/2}$–$2s^22p^5\ ^2P_{1/2}$) and Fe XIX λ1118.07 ($2s^22p^4\ ^3P_2$–$2s^22p^4\ ^3P_1$), arising from transitions within the ground configurations of the atom. The observed wavelength of the Fe XVIII λ974.85 transition (corrected for the +12.3 km s^{-1} radial velocity of the star) agrees with the laboratory wavelength to 0.015 Å and confirms that the feature corresponds to the photospheric velocity. The FWHM equals 0.29 ± 0.02 Å, which is comparable to the thermal broadening expected in a plasma at $T = 10^{6.8}$ K. The line flux is measured to be $(3.6 \pm 0.4) \times 10^{-14}$ ergs cm^{-2} s^{-1}. These parameters, here measured from the photon (counts) spectrum, confirm the values in Redfield et al. (2003). The Fe XIX transition appears blended with a broad C I multiplet that occurs from 1117.2 to 1118.5 Å. The blend was deconvolved into a broad (FWHM = 1.4 Å) and narrow (FWHM = 0.33 Å) component. Line center, corrected for the stellar radial velocity and corrected by using the Si III transition at 1113.228 Å as a fiducial reference, occurs at 1118.081 Å, in agreement within 0.01 Å with the laboratory value. The expected fluxes of Fe XVIII and Fe XIX from β Cet were predicted by using atomic emissivities from CHIANTI/APEC (Dere et al. 2001; Smith et al. 2001) and an emission measure distribution from iron lines measured in the *EUVE* spectrum in 2000 (Sanz-Forcada et al. 2002); the observed fluxes in *FUSE* spectra are stronger than the predictions by a factor of ∼1.7 for λ974 and by a factor of 1.6 for λ1118. The ratio of the fluxes of Fe XVIII/Fe XIX is predicted to be λ974/λ1118 = 1.8, as compared to the measured value of 2.02, an amount that is within 12% of the prediction.

The agreement of the flux values within a factor of 2 is considered acceptable, based on the uncertainties in atomic parameters, density effects, calibration errors, the interstellar absorption correction, and possible variations in the source itself. Because β Cet became much more active in 2000 August as compared to the earlier EUVE observation in 1994 and displayed frequent flaring activity not found earlier (Ayres et al. 2001b; Sanz-Forcada et al. 2003), this activity may have continued through the *FUSE* observations in 2000 December although we have no direct evidence of continued activity. Certainly, a variation of a factor of 2 in highly ionized species is not surprising, as has been noted earlier in Capella (Dupree & Brickhouse 1995). It is also possible that there is additional cascade contribution from higher levels of Fe XVIII and Fe XIX that is not included in the CHIANTI/APEC emissivities, leading to an underestimate of the predicted value.

5.2. *31 Com*

It appears likely that Fe XVIII and Fe XIX are also present in the spectrum of 31 Com. Star 31 Com has a high surface flux of O VI and an emission measure distribution derived from *EUVE* spectra that mimics that of β Cet (Sanz-Forcada et al. 2002), except that the coronal enhancement occurs at slightly higher temperatures. Using the *EUVE* emission measure distribution, the flux of Fe XVIII λ974 is predicted to be 1.8×10^{-15} ergs cm^{-2} s^{-1}, and Fe XIX λ1118 is estimated as 1.63×10^{-15} ergs cm^{-2} s^{-1}. Although weak,[6] Fe XVIII is observed in the SiC2A channel with a flux of 4.6×10^{-15} ergs cm^{-2} s^{-1}, 2.5 times larger than predicted. The Fe XIX flux is difficult to measure because it is located in a complex of C I emission. To estimate the flux, we scaled the expected C I strength in the blended multiplet at 1118 Å in 31 Com from the adjacent C I multiplet near 1115 Å using the ratio measured in the quiet-Sun spectrum (Curdt et al. 2001). The

[6] In addition to intrinsic weakness, the Fe XVIII is affected by the C III λ977 broad wing that contributes to elevate the background. Taking the binned spectrum, we fit multiple Gaussian profiles to the C III wing, Fe XVIII, and nearby airglow lines, as well as the linear continuum. The FWHM of the Fe XVIII emission was determined as ∼0.40 Å, and so the summing of the spectrum was made to ∼1.65 σ, which should include ∼90% of the line emission for the Fe XVIII feature.

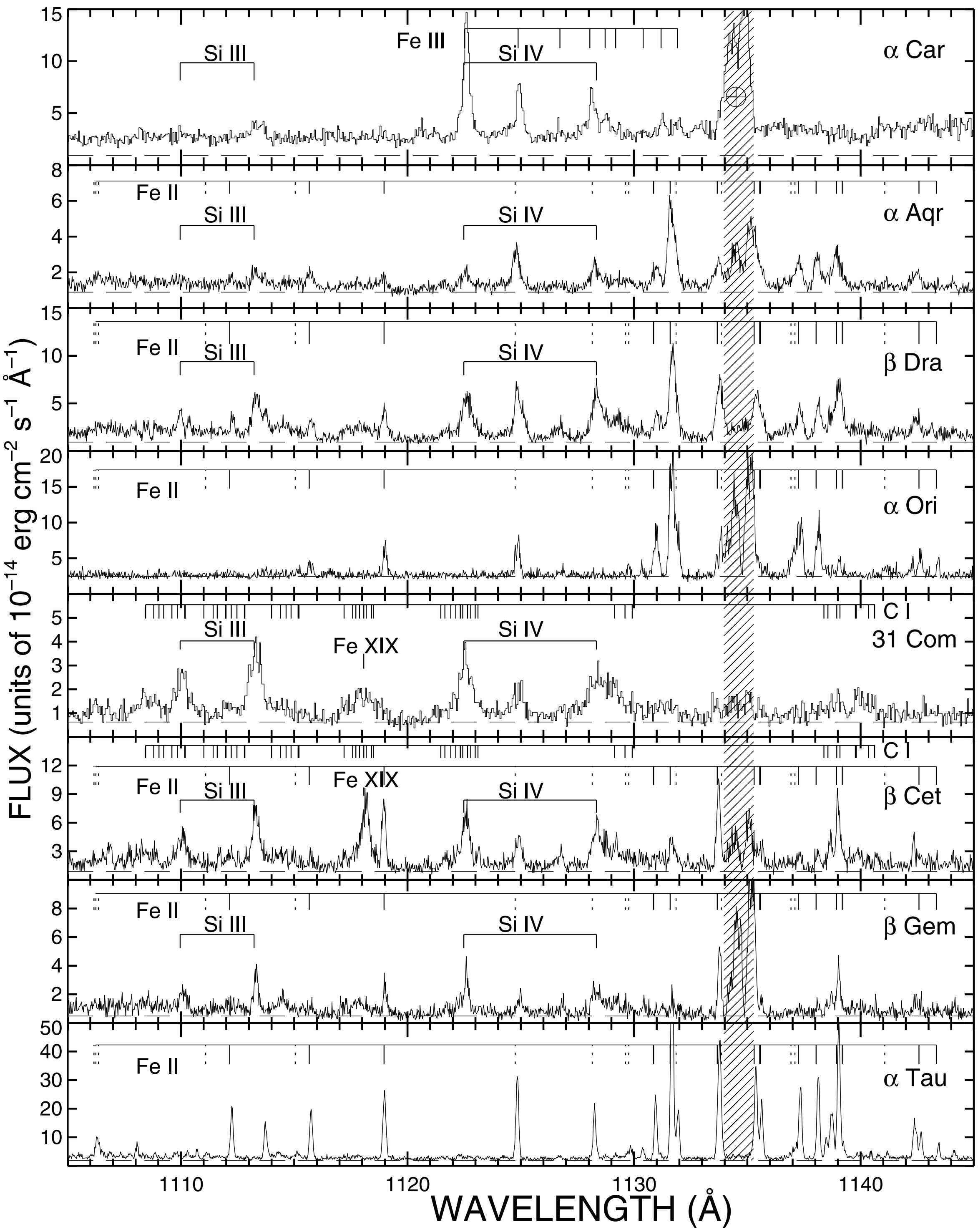

Fig. 4.—Region 1110–1145 Å showing the presence of fluorescent Fe ii emission in many of the coolest targets. The hatched area marks the position of N i airglow emission. The location of Fe ii emission marked by solid (dashed) lines indicates those features pumped by radiation within (larger than) 1.8 Å of the H Lyα core and might be expected to be strong (weak).

cell center and network ratio differ only by 7%. Fe xix observed in the LiF2A channel equals 6.62×10^{-15} ergs cm^{-2} s^{-1}. As in the case of β Cet, the observed *FUSE* values are larger than predicted, in this case by a factor of 4. The flux ratio Fe xviii/Fe xix is predicted to be 1.1 as compared to the observed value of 0.7, representing a difference of a factor of 1.6. Such a discrepancy is not surprising considering the flux extraction procedure in addition to other uncertainties noted above.

6. LYMAN SERIES EMISSION

All of the stars display an Lyβ emission feature at 1025 Å. This is the strongest airglow line in the *FUSE* spectral range and is present in both day and night spectra. Unfortunately, the strong airglow has caused a drop in the gain of the detectors in this wavelength region when using the large aperture. Because the reported *x*-positions of the photons arriving on the detector

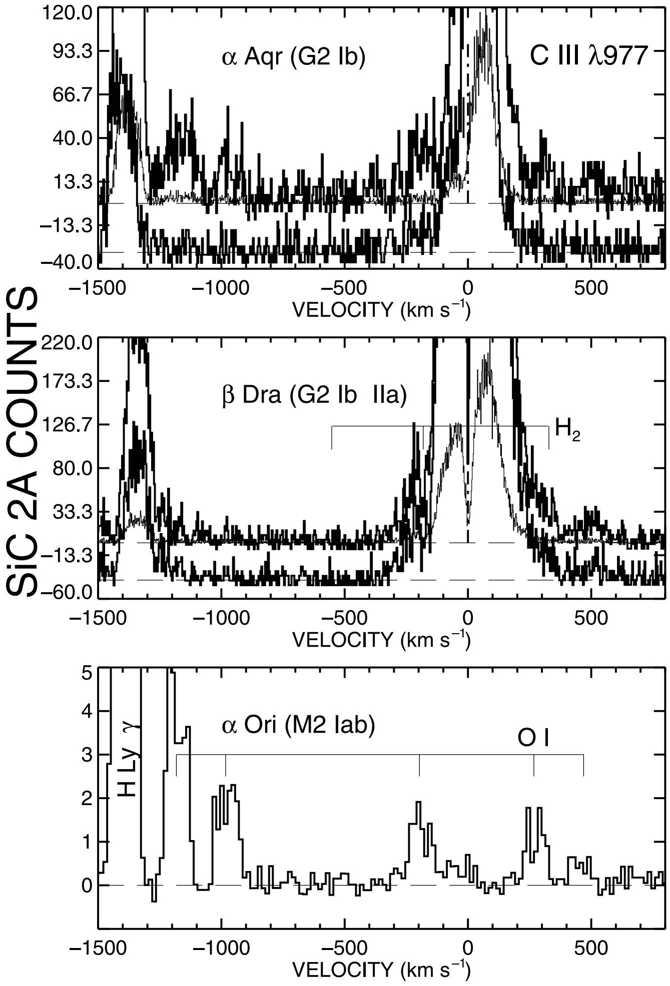

FIG. 5.—Identification of weak features, here in the wings of C III λ977, allowed by the extremely low background of the *FUSE* detectors. Total (*upper curve*) and night-only (*lower curve, offset*) extractions are shown for α Aqr and β Dra. These rebinned spectra are shown at 10 times the original count level. The original profile is also displayed (*thin line*). Airglow lines of H Lyγ are present in all spectra. The airglow due to O I is present in α Ori and α Aqr and very weak, if not absent, in the β Dra spectrum. Emission near +500 km s^{-1} in the spectrum of β Dra is present in both total and night extractions, demonstrating the ability of *FUSE* to detect such weak features. It appears likely that this emission results from O I λ978.624 that is fluoresced by the stellar C III line itself via O I transitions sharing the same upper level, $2p^35s\ ^3S_1$. H_2 may also contribute to the absorption feature near -200 km s^{-1} in β Dra; the location of three H_2 transitions is marked as synthesized by H2ools.

are a function of the gain, the drop in gain (“gain sag”) causes lower gain events to be incorrectly positioned (see the *FUSE* Instrument and Data Handbook, version 2.1, § 9.1.12). The tendency for photons to be moved to shorter wavelengths on the LiF1A detector causes emission features to appear that can mimic actual stellar emission. The nature of the observed emission is revealed by inspection of the pulse-height distribution of the feature in the raw data and extraction of the spectrum with CalFUSE using various levels of the pulse-height screening parameter. Emission features on the short-wavelength side of Lyβ in Figure 6 become weaker when the pulse-height threshold is raised. The *FUSE* project remedies the gain sag problem periodically, but it is usually present at some level, making suspect the emission features that lie shortward of Lyβ.

In most of our targets there is excess emission to the *long*-wavelength side of Lyβ (Fig. 6). To identify the stellar emission in this complex feature, the profiles are compared to *FUSE* reference airglow spectra. An extended exposure on the “sky” was taken in 1999 August yielding spectra through all *FUSE* apertures with no target in the field. Because this date was very early in the *FUSE* mission, the profiles are not affected by gain changes in the detectors. These spectra are available on the *FUSE* Web site, and the LiF1A spectra were scaled to the observed airglow profile in the target stars. Spectra from the LWRS were used for all stars, except for α Tau, where an MDRS spectrum was substituted. The profile of the Lyβ airglow emission is the same for both day and night extractions, although the flux level is lower in spectra obtained at night. While absorption by interstellar deuterium is expected at 1025.443 Å, airglow in the large aperture contaminates this region. Spectra of α Tau, taken through the medium aperture, do not have sufficient signal to detect D I absorption.

All of the targets except α Ori have excess emission on the long-wavelength side (Fig. 6) that arises from H I in the stellar chromosphere. Emission is expected and likely to be self-reversed because Lyβ is an optically thick chromospheric line. Additionally, motion in the atmosphere can create asymmetries in the profiles, and absorption by interstellar hydrogen can substantially change their appearance. It is not possible to draw conclusions about the intrinsic stellar line flux or shapes because of airglow contamination and instrumental effects. The H Lyβ profile of α Tau, because it was taken through the MDRS, reducing the airglow contamination, comes closest to sampling the stellar profile, but the interstellar absorption at -30 km s^{-1}, coupled with the stellar radial velocity of +54 km s^{-1}, affects the central reversal. In spite of problems with the line core and blue wings, the extent of the H Lyβ long-wavelength emission wings indicates the width of the H Lyα profiles. The H Lyβ stellar emission wings on the long-wavelength side span a region 0.5–1.0 Å. Because the H Lyα line width is about a factor of 1.4 broader than the H Lyβ line in the Sun (Lemaire et al. 2002), it appears that sufficient flux is present in the stellar H Lyα wings to pump Fe II and cause fluorescence observed in the spectra shown in Figure 4. The fact that α Ori does not show any stellar emission in Lyβ may provide the explanation for the weakness of the fluoresced Fe II emission line near 1135 Å noted earlier in § 4.

7. TIME VARIATION: β CETI

One star in our sample, β Cet, showed substantial flux variation during the exposure. Light curves (Fig. 7) were created by considering the raw, time-tag *FUSE* data. Each of the 10 β Cet exposures was combined into a single time-tag file using the TTAG_COMBINE routine in the *FUSE* software. The detector image from this combined data set was inspected and an area bounding the emission line selected. Another area of the same size lying either above or below the spectrum was also selected to estimate the level of the detector background.

For each area, the number of photons arriving in 100 s time bins was determined throughout the observation. The O VI light curve was created from the LiF1A and LiF2B λ1032 lines, while the C III light curve was created from the λ977 lines in the SiC1B and SiC2A channels summed with the λ1176 lines from the LiF1B and LiF2A channels.

The C III and O VI light curves show the same features, namely, a rise in the fluxes of the lines by around 50% during the observation, followed by a fall to the original flux level at the beginning of the exposure. The rise and fall times are comparable at $\sim$20 ks each. The increase in flux of the λ1032 line is simply due to a broadening of the line profile as illustrated in Figure 8. The flux at the center of the line remains constant, and the added emission arises at both high and low velocities from line center

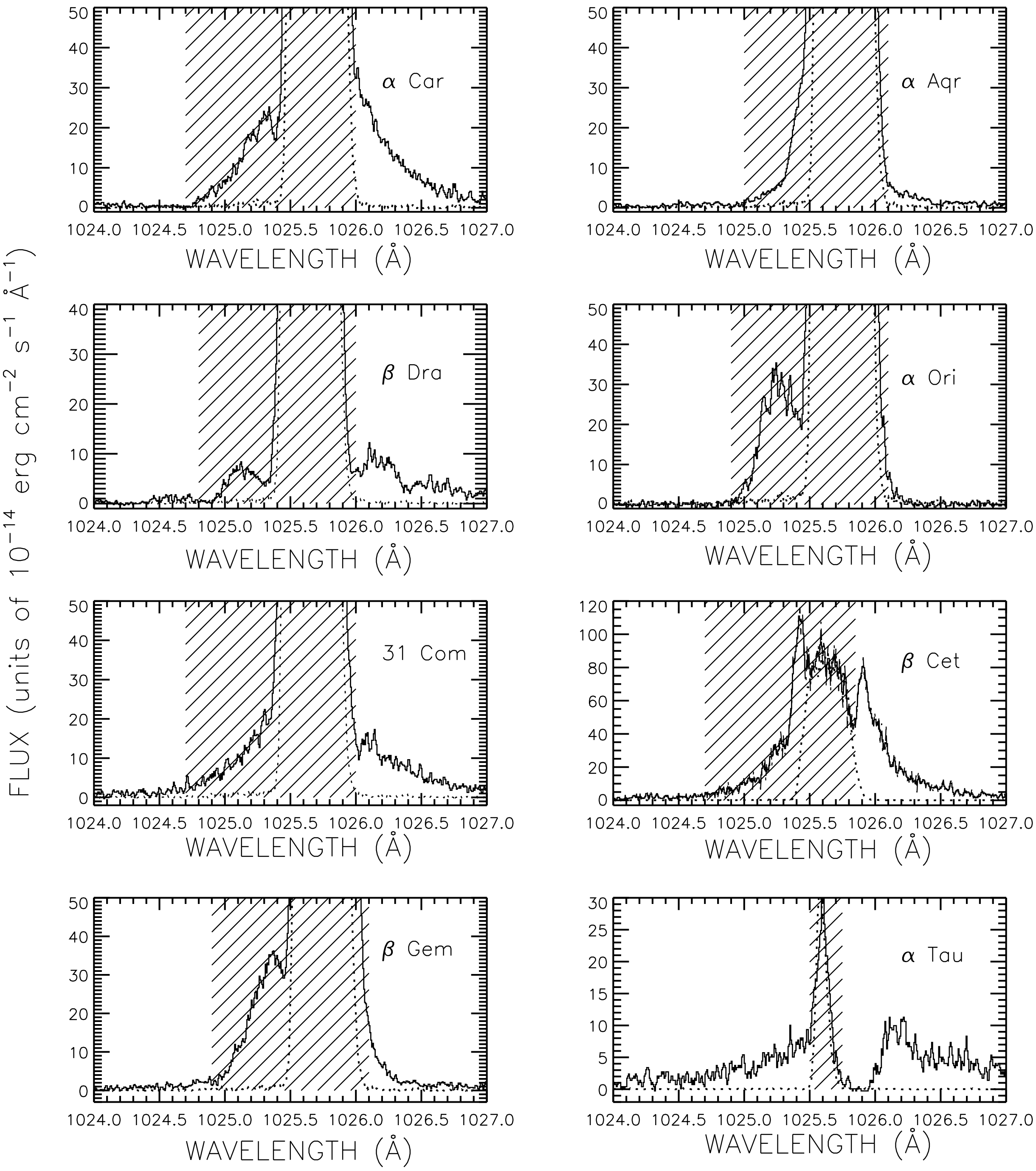

Fig. 6.—Lyβ profile in the target stars from the total (day + night) exposures in LiF1A. A scaled spectrum of the Lyβ airglow profile taken in 1999 August through the LWRS or MDRS, as appropriate, is shown in each panel (*dashed line*). The hatched area indicates where spectra are most likely affected by airglow and detector walk caused by gain sag (see text). Excess emission from the stars on the long-wavelength side of the Lyβ profile appears in all targets except α Ori. Note the narrow appearance of the Lyβ airglow through the medium aperture (MDRS) in the α Tau spectrum. With this aperture, detector walk has not occurred. The night-only extraction shows little difference on the long-wavelength wing from the total data but is noisier because of the shorter exposure. Data for β Cet are only nighttime exposures.

(Fig. 8). Three other flaring events observed in O vi with *FUSE* exhibited different profiles. AB Dor had a redshifted emission component in O vi that extended to 600 km s^{-1} (Ake et al. 2000). During flares from AU Mic an *enhanced* core appeared in O vi, in addition to broad wings (in one flare) or redshifted emission (in another flaring event; Redfield et al. 2002). Thus, this β Cet event remains unique with its symmetric broadening and constant core.

Coronal emission in β Cet measured with *EUVE* exhibited flaring events during 2000 August (Ayres et al. 2001b; Sanz-Forcada et al. 2003); however, they lasted longer than 1 day. Star β Cet is a slow rotator ($v \sin i = 4$ km s^{-1}; Fekel 1997) so the O vi enhancement does not appear related to the passage of active regions across the disk and most likely represents a long chromospheric transition region flaring episode.

Many stars exhibit rapid flux increases in transition region lines of Si iv and C iv. However, these flares typically have rise times on the order of a few minutes or less (cf. the dwarf stars AD Leo [Bookbinder et al. 1992], AB Dor [Gómez de Castro 2002], and AU Mic [Robinson et al. 2001]). The active dwarf binary HR 1099 showed a rise time of about 1.5 hr in one event (Ayres et al. 2001a), but no events comparable to the 5.5 hr rise observed here.

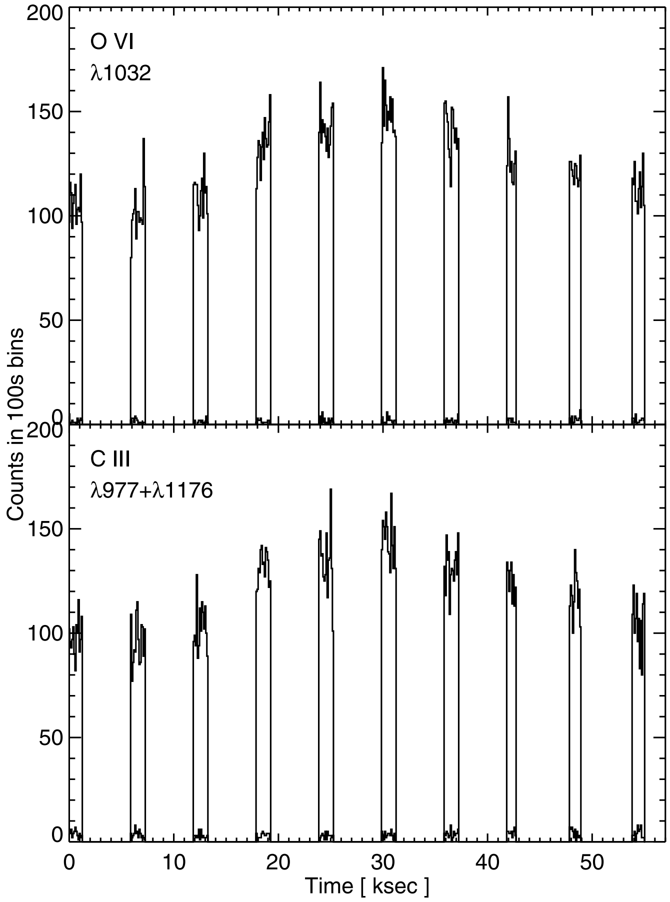

FIG. 7.—Light curves for O VI (*top*) and C III (*bottom*) during the observation of β Cet. The data have been placed into 100 s time bins as described in the text. In each panel the light curves for the background level are also shown, demonstrating the low background levels of *FUSE*.

An RS CVn–type binary, λ And, did undergo ultraviolet flaring (Baliunas et al. 1984) in an event that lasted for about 5 hr. Although most normal single giants have not shown transition region flaring, the bright giant λ Vel (K4 Ib–II) and β Cet have exhibited coronal flare episodes lasting from minutes to days (Ayres et al. 1999, 2001b; Sanz-Forcada et al. 2002). It is plausible that the enhancement of β Cet in the transition region lines corresponds to such a coronal event detected in these other stars.

A few transition region line profiles have been measured during stellar flares, but no consistent pattern emerges. The flare star AD Leo showed a substantial (up to 1800 km s^{-1}) redshift in its C IV λ1550 emission during a flare (Bookbinder et al. 1992). In HR 1099, broad and narrow components of transition region lines of Si III, Si IV, C IV, and N V remained present, but the flux of one or the other component increased in flares (Ayres et al. 2001a). In AU Mic, a single broad line of Si IV appeared that alternately became shifted toward longer and shorter wavelengths during a flare (Linsky & Wood 1994). Another flare in AU Mic showed no change in the Si III line profile but simply a flux enhancement (Robinson et al. 1992). Line profiles during flares in the active rapidly rotating dwarf, AB Dor, are not always the same but frequently show redshifts (Gómez de Castro 2002; Ake et al. 2000), although rapid broadening of the C IV lines to several hundred kilometers per second is observed in the strongest flares. The broadening of the β Cet profile is within the range of diverse profiles found in other stars during flares, but the rise time appears anomalously long.

8. DENSITY DIAGNOSTICS

The *FUSE* region contains two strong transitions from C III, $\lambda\lambda$977 and 1176, whose ratio is principally sensitive to electron density in optically thin plasmas over the range 10^8–10^{11} cm^{-3} (Dupree et al. 1976). These transitions have been widely utilized in solar studies and more recently in dwarf stars using *FUSE* spectra (see Redfield et al. 2002). However, if one or both of the lines are optically thick, a simple ratio diagnostic cannot be used. Signs of optical depth in the stellar λ977 line were first noted in several targets from *ORFEUS* spectra indicated by anomalous widths and relative fluxes (Dupree & Brickhouse 1998). Spectra from *HST* and *FUSE* illustrate optical depth effects as well (Del Zanna et al. 2002; Redfield et al. 2002). *FUSE* spectra of luminous stars reveal not only asymmetries in the λ977 line (see § 11.2 and Fig. 9), but signs of anomalous ratios among components of the λ1176 multiplet too (see Fig. 10). As compared to the profile in the quiet Sun, this multiplet is compromised by optical depth effects. The profiles of λ1176 in the

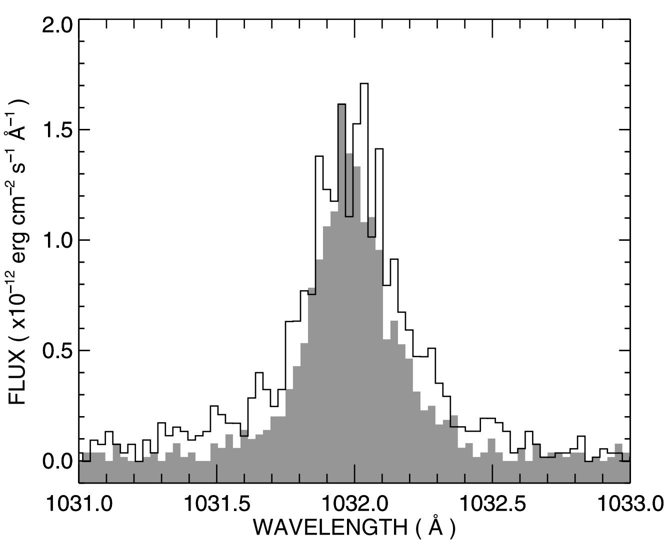

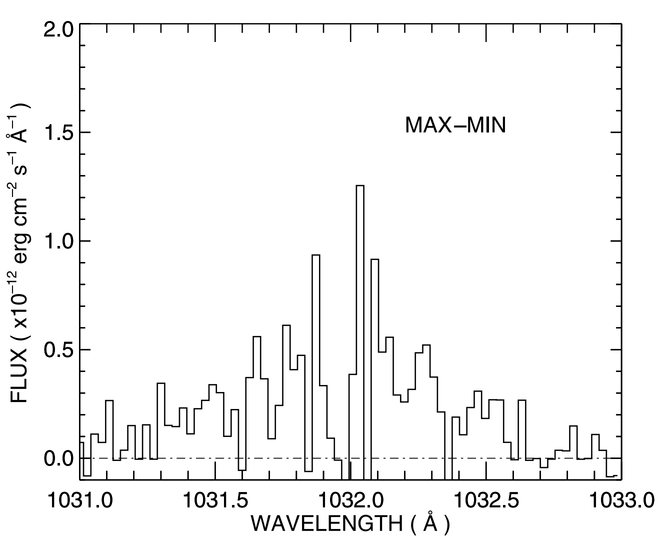

FIG. 8.—*Left*: Comparison of O VI λ1032 profiles from the first (*shaded*) and sixth β Cet exposures, corresponding to the minimum and maximum of the light curve, respectively. It can be seen that the increase in flux is due to a broadening of the line profile. *Right*: Difference between the O VI profiles at maximum and minimum light, illustrating the appearance of emission about $\pm$0.2 Å (about $\pm$60 km s^{-1}) from line center while emission at line center remains effectively constant.

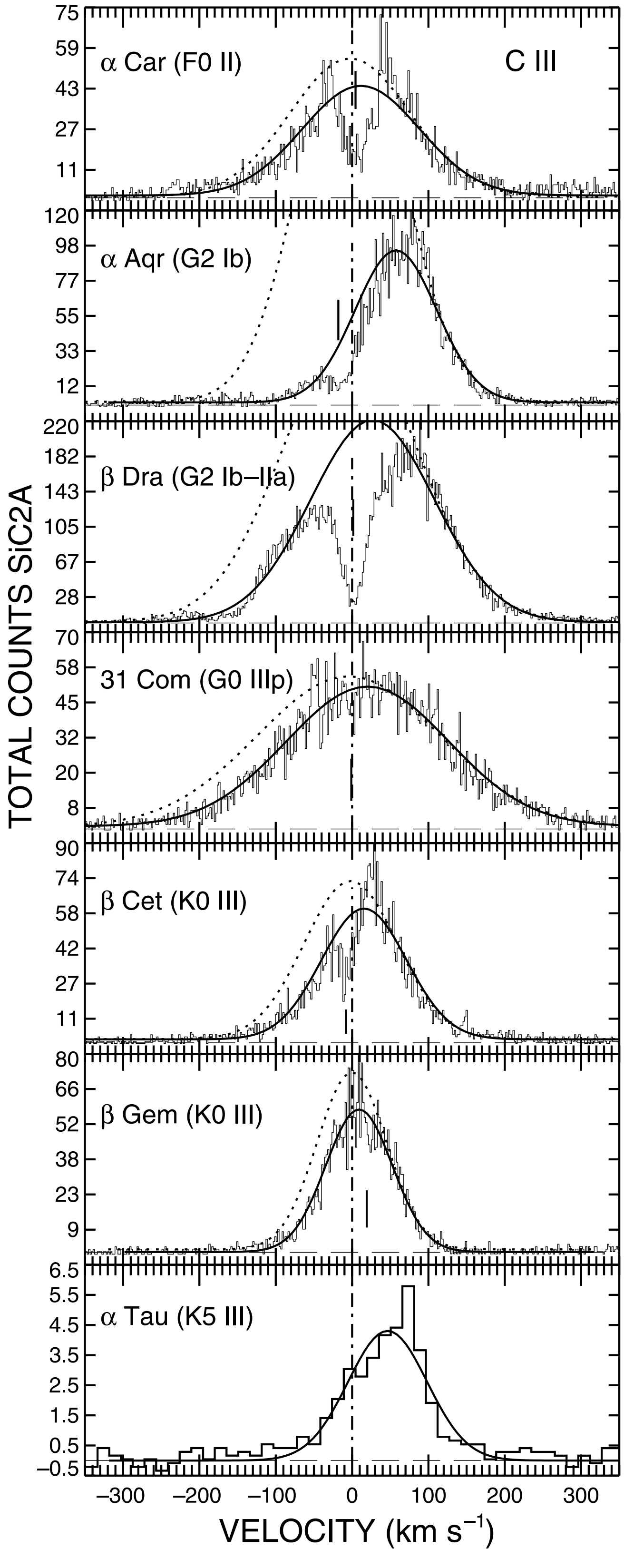

FIG. 9.—C III λ977.020 emission in the target stars as measured in the SiC2A channel. The zero point of the photospheric velocity scale is indicated by a dot-dashed line. Single Gaussians have been fitted to the profiles (*solid line*) and to the positive velocity side of the profiles (*dashed line*). A short solid line marks the position of the interstellar C III absorption. Line profiles are not rebinned or smoothed except for α Tau, which is rebinned by 8 pixels. C III emission is detected in all targets and appears not to be symmetric in most but exhibits absorption at negative velocities. The *FUSE* wavelength scale was used for α Tau.

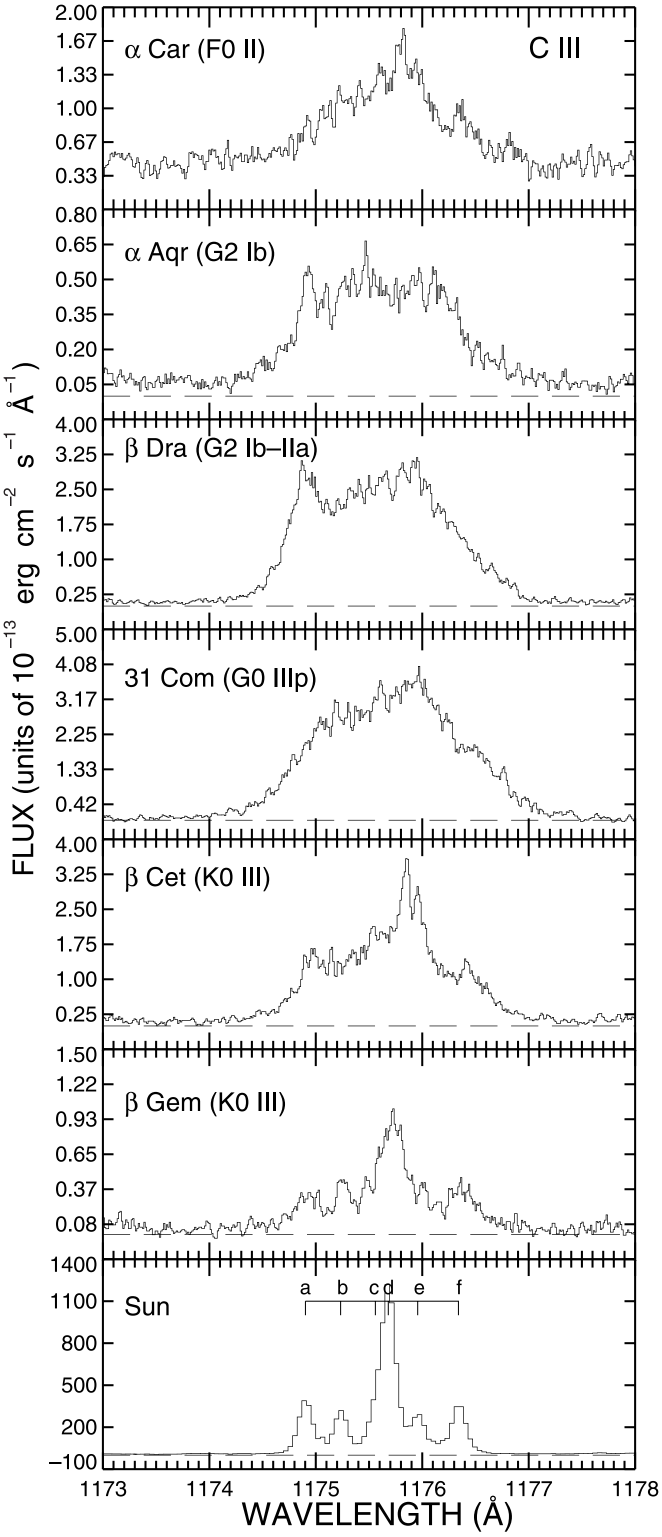

FIG. 10.—C III λ1176 multiplet in the target stars as measured in the LiF2A channel. A solar sunspot spectrum (Curdt et al. 2001) is shown in the bottom panel. The six components of the multiplet are marked *a–f*.

TABLE 6
GAUSSIAN FITS TO PHOTON SPECTRUM OF C III λ977

Star	Gaussian Fit (Single) Vel$_{center}$ (km s^{-1})	FWHM (km s^{-1})	Flux$_{Gauss}$[a] (ergs cm^2 s^{-1})	Gaussian Fit (Long-λ Side) Vel$_{center}$ (km s^{-1})	FWHM (km s^{-1})	Flux$_{Gauss}$[a] (ergs cm^2 s^{-1})
β Cet	+15.6 ± 3.1	131 ± 2	(6.02 ± 0.6)E−13	−1.85 ± 3.0	143 ± 2	(7.98 ± 0.8)E−13
α Tau[b]	+10.9 ± 6.0	100 ± 10	(5.70 ± 0.6)E−15	...	...	...
α Car	+11.6 ± 0.9	180 ± 3	(3.60 ± 0.4)E−13	−2.60 ± 2.5	184 ± 3	(4.72 ± 0.5)E−13
β Gem	+9.10 ± 1.5	106 ± 2	(2.75 ± 0.3)E−13	−0.28 ± 1.5	102 ± 2	(3.58 ± 0.4)E−13
31 Com	+20.3 ± 1.5	250 ± 4	(1.04 ± 0.1)E−12	−4.30 ± 2.0	281 ± 4	(1.26 ± 0.2)E−12
β Dra	+26.9 ± 1.3	190 ± 3	(1.96 ± 0.2)E−12	−2.80 ± 4.0	207 ± 4	(2.99 ± 0.3)E−12
α Aqr	+57.5 ± 2.1	126 ± 2	(2.70 ± 0.3)E−13	−0.67 ± 3.0	157 ± 2	(8.52 ± 0.9)E−13

NOTE.—Gaussian profiles fitted to stellar emission profile from SiC2A channel in photons (counts) using Poisson statistics (see text).
[a] Fluxes as measured from the Gaussian fit; should be used for relative contribution only.
[b] Single Gaussian fit to rebinned data.

stars are generally not dominated by the central component (λ1175.709, $2s2p\ {}^3P_2$–$2p^2\ {}^3P_2$) of the six transitions forming the multiplet as they are in the Sun. The central transition shows the greatest effect of optical depth where, near the solar limb, it becomes weaker by as much as a factor of 2 (Doyle & McWhirter 1980). Only in the *FUSE* spectrum of β Gem does the λ1176 profile appear to be optically thin; however, there are signs from profile fitting and bisections that the λ977 transition in this star is not optically thin. We conclude that the λ1176/λ977 multiplet ratio cannot be applied to infer electron density in the chromospheres of these luminous stars.

The relative strengths of certain members of the λ1176 multiplet can indicate electron density if they can be separated. The 2–2 transition (λ1175.709) is the strongest, and in the optically thin case its ratio (or the ratio of the blend of λ1175.709 [line *d*] and λ1175.587 [line *c*]) relative to λ1175.983 (line *e*) is sensitive to density over the range 10^8–10^{10} cm^{-3}. Excluding the strongest line from the multiplet, the ratio of λ1175.983 (line *e*) to λ1175.260 (line *b*), λ1175.587 (line *c*), or λ1176.367 (line *f*) could be used if sufficient signal is available; they are also sensitive to density between 10^8 and 10^{10} cm^{-3}. Only β Gem appears to have an optically thin multiplet in which these ratios can be used. Using a profile of λ1176 from the combined LiF2A and LiF1b segments for β Gem, we fit the six components of the multiplet simultaneously with Gaussians by adopting the laboratory wavelength separations and holding all lines in the multiplet to the same FWHM. The line ratios, $e/(c+d)$, e/c, e/b, and e/f, set a lower limit on the electron density of 10^9 cm^{-3} for a temperature $T = 80{,}000$ K using rates from CHIANTI (Young et al. 2003). Spectra with longer exposure times are needed to constrain a high-density limit.

9. PROFILE FITTING

Because some emission lines from cool stars do not appear Gaussian in shape, a practice (Wood et al. 1997) has developed to invoke multiple Gaussian components to characterize the line profiles. The C III λ977 and O VI λ1032 lines are the strongest stellar emission lines in these spectra and most amenable to multiple component fits. Our line-fitting procedure is applied directly to the spectrum of photon counts because this technique enables proper assessment of errors.

The reason for a preference for photon fitting derives from the characteristics of the spectrum and the *FUSE* detectors. The background level of *FUSE* spectra is extremely low and, coupled with the intrinsically low continuum levels of cool stars, results in the spectra containing typically 0–2 counts bin^{-1} outside of emission lines and in extended line wings. Measurement errors for such low count levels are not distributed according to Gaussian statistics, and so the minimization of χ^2 to derive emission-line parameters is not appropriate for such spectra (e.g., Nousek & Shue 1989).

The method employed here is to minimize the *C*-statistic (Cash 1979), which treats the statistics for small counts per bin data correctly. *C* is defined as

$$C = 2\sum_{i=1}^{N}[f(x_i;\ a) - n_i \ln f(x_i;\ a)], \quad (1)$$

where N is the number of data points, $f(x_i; a)$ is the function fitted to the data (dependent on parameters a), and n_i is the number of counts in bin i. In the present case the emission lines are treated as a superposition of one or more Gaussians and a linear background. Both background and lines are fitted simultaneously. Minimization of *C* is performed using Powell minimization through a routine available in IDL (*powell.pro*). Results of the fits for C III λ977 and O VI λ1032 are discussed below.

9.1. C III λ977

The C III λ977 line is affected by interstellar absorption or central reversals in several stars, and for these stars we omit from the fit those points affected by the absorption. The C III λ977 transition is fitted by a single Gaussian profile. All of these single Gaussians are shifted to longer wavelengths that, if representing coherent mass motions in the atmospheres, would suggest the presence of infalling material. If symmetric emission is simply shifted to longer wavelengths, the infalling emission region must arise from the whole atmosphere behaving coherently. Of course, stars can have complex surface structures with an uneven distribution of regions of activity that produce departures from symmetry in the line profiles. In solar magnetic structures, a restricted emission region produces profiles characterized by redshifts in transition region lines (Doschek et al. 1976; Teriaca et al. 1999; Peter & Judge 1999),[7] although anomalous center-to-limb behavior suggests that other mechanisms are present (Achour et al. 1995 and references therein). Dwarf stars also show redshifted emission in transition region

[7] The SUMER spectrograph on the ESA/NASA *Solar and Heliospheric Observatory* (*SOHO*) mission, used for most of these measurements, has lower spectral resolution than *FUSE*: a 2 pixel element covers ~0.09 Å or $R \sim 12{,}000$ so that detailed shapes of the narrow solar emission line profiles cannot be measured.

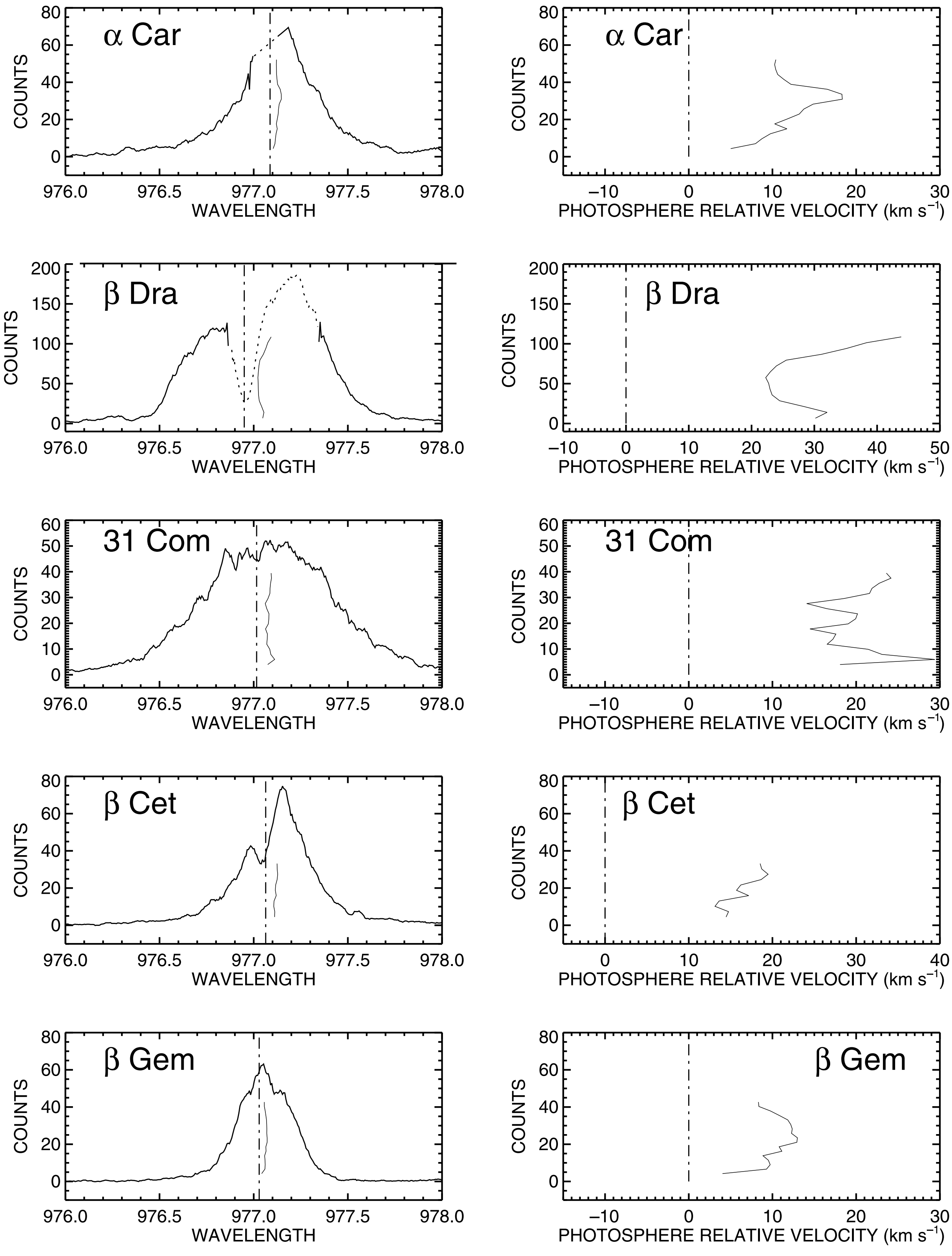

FIG. 11.—Bisector of the C III λ977.920 emission in five targets. The stellar profiles and bisectors are shown in the left panels, and the positions of the bisectors are given on a velocity scale in the right panels. Note that the bisectors do not extend below 5 counts so as not to be affected by possible weak airglow emission. The dashed line in α Car and β Dra profiles indicates the region omitted from the bisector process. H_2 absorption on the short-wavelength side of β Dra compromises the bisector below $\sim$50 counts. Errors in centroiding are less than 2 km s^{-1}. Star α Aqr is not included because the line is obviously absorbed on the short-wavelength side (see Figs. 9 and 20).

lines (Wood et al. 1997; Redfield et al. 2002). In the luminous giant and supergiant stars observed with *FUSE*, it appears more likely to assume as a working hypothesis that there is opacity in the C III λ977 line resulting from outflowing material and causing the appearance of a redshift. Radiative transfer effects (Hummer & Rybicki 1968) can cause the appearance of a redshifted profile resulting from increased opacity on the blue side of the line. Semiempirical models of luminous stars have demonstrated such asymmetries in chromospheric line profiles (e.g., Lobel & Dupree 2001).

The presence of such opacity can be investigated by fitting a Gaussian profile *only* to the long-wavelength wing of the line, eliminating from the fit both the peak emission and the short-wavelength side of the line profile from the peak to approximately -200 km s^{-1}. These wing fits are also shown in Figure 9, and parameters are listed in Table 6. The one-sided Gaussian fits predict a line center that is less than 5 km s^{-1} from the predicted photospheric velocity of all stars. The resultant fits are consistent with the idea that the observed profiles are asymmetric with the short-wavelength side of the profile subject to absorption.

For several targets, it is useful to further characterize these line profiles using a bisection technique. The bisector of a symmetric emission line should remain at constant wavelength (or velocity) for all parts of the profile. To determine the bisectors, the profiles were smoothed and cut into 25 segments, each of flux strength 1/25 of the profile peak. The weakest part of the profile ($\leq$5 counts) was not included. The centroid of each segment was determined omitting regions crossing the interstellar absorption feature. The resulting bisectors of the C III λ977 emission in five targets (Fig. 11) show that these profiles are not symmetric. Certain systematics are apparent from Figure 11. Toward the base of the lines the bisector shifts toward negative velocities that could arise from geometric blocking by the stellar disk at high positive velocities and/or decreased wind opacity at high negative velocities causing line emission to appear. In 31 Com, the core of the λ977 line itself appears asymmetric with enhancement at positive velocities, much like the O VI λ1032 profile in β Dra (see following text). Both profile fitting and bisectors suggest that opacity is present in the C III λ977 profile in all targets except α Tau, where the signal is weak.

9.2. O VI λ1032

The O VI λ1032.926 (Kaufman & Martin 1989) profile has extra emission in the wings of most targets, and as expected, two Gaussian curves appear to produce a better fit to the profile than a single curve (see Fig. 12 and Table 7). Centroids of the narrow and wide Gaussian appear coincident in α Car and β Dra, but they are separated in the remaining four targets where it can be measured. Three of these stars (β Gem, 31 Com, and α Aqr) show a narrow component that is shifted to longer wavelengths than the wide component. Star β Cet has the opposite shift: the narrow component is shifted to shorter wavelengths. The ratio of widths of wide:narrow varies between a factor of 1.7 and 2.9. The flux in the narrow component is generally larger by a factor of 1.1–2.6 than the flux in the broad component except for α Car (0.94) and α Aqr (0.40).

The physical interpretation of a two-Gaussian fit to λ1032 is not obvious (see § 11.2). Fitting the long-wavelength side of the profile with a single Gaussian is also shown in Figure 12 and Table 8 with the exception of α Tau. Evidence for absorption on the short-wavelength side appears in all cases. A line bisecting the smoothed O VI λ1032 profile (Figs. 13 and 14) demonstrates asymmetries in all stars. The line cores also merit notice. Line

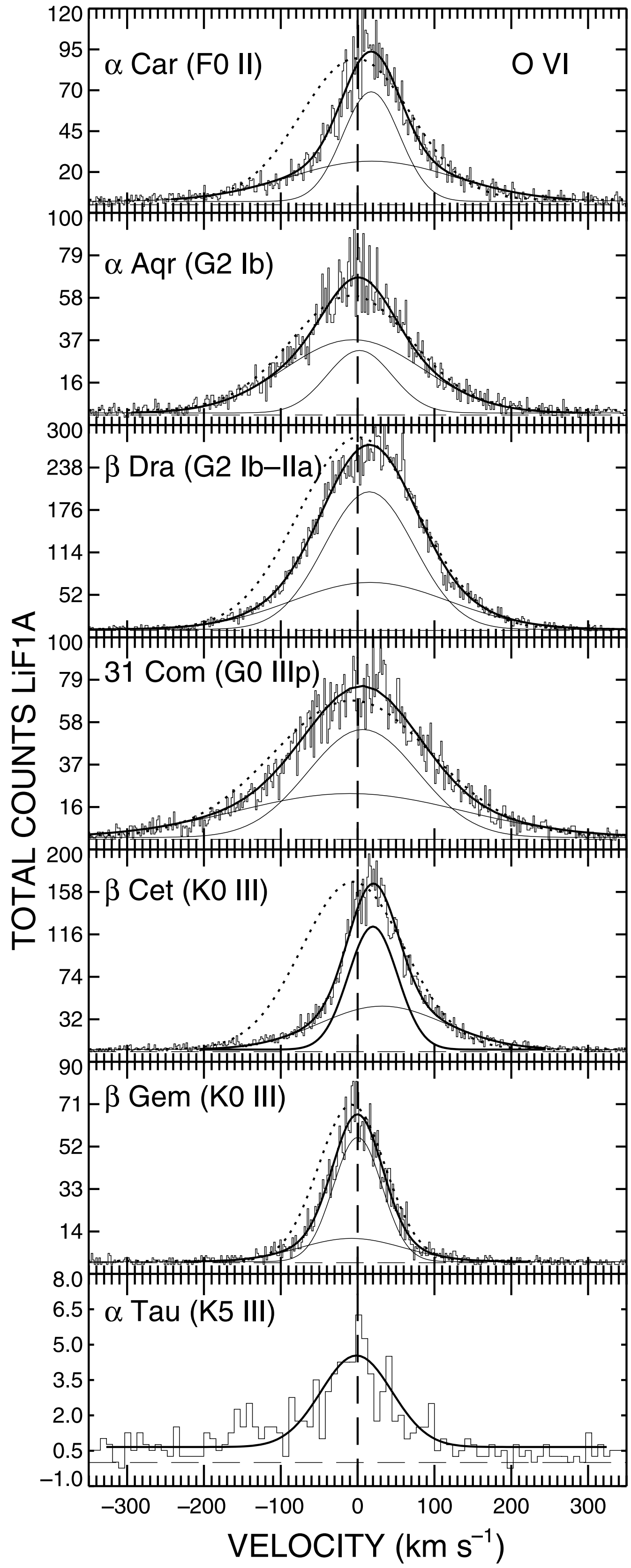

FIG. 12.—O VI λ1032 transition in the target stars. Except for α Tau, multiple Gaussians have been fitted to the line profiles (*thin solid lines*), and the sum is marked by a thick solid line. Single Gaussians have also been fitted to the positive velocity side of the profiles (*dotted line*) to display the intrinsic line asymmetries. The position of the stellar photosphere is marked by the dashed line at 0.

TABLE 7
Parameters of Two Gaussian Fits to O vi λ1032

Star	Two-Gaussian Fit (Narrow) Vel$_{center}$ (km s^{-1})	FWHM (km s^{-1})	Flux$_{Gauss}$[a] (ergs cm^2 s^{-1})	Two-Gaussian Fit (Wide) Vel$_{center}$ (km s^{-1})	FWHM (km s^{-1})	Flux$_{Gauss}$[a] (ergs cm^2 s^{-1})
β Cet	+20.0 ± 1.8	75 ± 2	(2.87 ± 0.3)E−13	+32.1 ± 2.0	191 ± 10	(2.58 ± 0.3)E−13
α Tau[b]	−1.45 ± 2.0	182 ± 6	(2.47 ± 0.2)E−14	...	...	...
α Car	+17.6 ± 2.0	87 ± 3	(1.02 ± 0.1)E−13	+18.4 ± 3.1	253 ± 15	(1.09 ± 0.1)E−13
β Gem	+0.142 ± 1.5	75 ± 2	(7.57 ± 0.8)E−14	−7.76 ± 2.1	157 ± 15	(2.96 ± 0.3)E−14
31 Com	+6.77 ± 1.5	168 ± 8	(2.75 ± 0.3)E−13	−9.89 ± 2.0	344 ± 20	(2.29 ± 0.2)E−13
β Dra	+15.2 ± 2.0	137 ± 5	(4.97 ± 0.5)E−13	+16.2 ± 1.9	239 ± 15	(2.95 ± 0.3)E−13
α Aqr	+2.48 ± 1.5	99 ± 4	(2.79 ± 0.3)E−14	−5.46 ± 2.0	210 ± 10	(6.91 ± 0.7)E−14

Note.—Gaussian profiles fitted to stellar emission profile from LiF1A in photons (counts) using Poisson statistics (see text).
[a] Fluxes as measured from the Gaussian fit; should be used for relative contribution only.
[b] The O vi profile does not have sufficiently good statistics to attempt a fit of two Gaussian profiles.

center, where the optical depth is largest, might be expected to show the first signs of opacity. Stars β Dra and 31 Com show the greatest velocity variation of the bisector at the peak of the profile. The cores are asymmetric with extra emission on the long-wavelength side. We suggest that this is another sign of opacity and outflow.

Information is provided by a direct comparison of members of the O vi multiplet. Since oscillator strengths of λ1032/λ1037 are in the ratio 2:1, the λ1032 line has a larger optical depth than λ1037. Overlaying the actual λ1032 profile (divided by 2) on the λ1037 spectrum, we find that the short-wavelength wing of λ1032 lies *below* the corresponding short-wavelength side of the λ1037 profile (except for β Dra, which has substantial H_2 absorption). This lends additional support to the presence of opacity in O vi.

10. H_2 ABSORPTION

The weaker component of the O vi multiplet, λ1037.617, is shown in Figure 15. Nearby is C ii emission. The scaling of the two Gaussian fits to the λ1032 line, reduced by a factor of 2 representing the optically thin ratio, gives a reasonable fit to the λ1037 emission although usually differs in detail. This procedure illustrates the presence of absorption by interstellar H_2 near the λ1037 line in the spectra of β Dra and α Aqr (Fig. 15). The corresponding H_2 transitions are shown in the appropriate panels of Figure 15. The position of H_2 absorption was computed from the files made available by S. R. McCandliss as H2ools on the *FUSE* Web site,[8] for a column density of 10^{18} cm^2, $T = 100$ K, and $b = 5$ km s^{-1} (McCandliss 2003). It is not surprising that these two stars in our sample, being among the most distant, show evidence of H_2 absorption. These two stars are near the plane of our Galaxy and located in the single sector where H_2 absorption has been detected by *FUSE* in the spectra of white dwarfs between 100 and 200 pc distant (Lehner et al. 2003). Lehner et al. (2003) suggest that the H_2 in the local interstellar medium may occur as one large diffuse cloud, possibly an extended thin sheet.

TABLE 8
Parameters of Single Gaussian Fit to O vi λ1032

Star	Gaussian Fit (Long-λ Side) Vel$_{center}$ (km s^{-1})	FWHM (km s^{-1})	Flux$_{Gauss}$[a] (ergs cm^2 s^{-1})
β Cet	−5.85 ± 10	156 ± 5	(7.82 ± 0.8)E−13
α Car	−1.99 ± 15	167 ± 10	(3.53 ± 0.4)E−13
β Gem	−7.55 ± 6	102 ± 5	(1.27 ± 0.1)E−13
31 Com	−7.02 ± 15	243 ± 15	(5.49 ± 0.5)E−13
β Dra	+1.38 ± 10	182 ± 8	(9.12 ± 0.9)E−13
α Aqr	−8.10 ± 8	189 ± 9	(9.68 ± 1.0)E−14

Note.—Gaussian profile fit to long-wavelength side of stellar emission profile from LiF1A in photons (counts) using Poisson statistics (see text).
[a] Fluxes as measured from the Gaussian fit; should be used for relative contribution only.

11. DISCUSSION

FUSE spectra show that warm atmospheres, with temperatures up to and including 300,000 K (the temperature of formation of O vi), are present in all stars, except the M supergiant, α Ori (see Fig. 1). Star α Tau is particularly interesting because X-rays have not been detected from this star (Hünsch et al. 1996), yet there is clearly high-temperature (3×10^5 K) plasma in the atmosphere. By analogy with solar coronal holes, the coronal temperature could be less where the high-speed wind originates and a high-temperature stellar corona might not be present where there is a strong wind. The supergiant α Ori is an obvious extreme example. In the Sun, the underlying energy flux is comparable between closed and open magnetic regions (Withbroe & Noyes 1977), but in open regions, the energy goes into driving the wind and not into heating the atmosphere.

11.1. *Systematic Flux Variations*

The surface fluxes of the C iii and O vi lines for each star were calculated using the Barnes-Evans relationship (Barnes et al. 1978) between $V-R$ color and surface brightness. The surface fluxes decrease systematically toward lower effective temperatures (Fig. 16). The C iii and O vi fluxes are tightly correlated (see Fig. 17) and, by contrast, the X-ray flux exhibits more variation, suggesting different heating mechanisms. The decay of the transition region lines appears similar to that of C iv in many giant stars and distinct from the chromospheric Ca ii behavior (Fig. 18). The rapid decay of the transition region emissions (C iii, C iv, and O vi) with temperature is reminiscent of models of magnetic dynamo behavior (Rutten & Pylyser 1988; Dupree et al. 1999) in contrast to acoustic models (Buchholz et al. 1998).

The enhancement of surface emission of the transition lines in 31 Com, a rapidly rotating giant, over that in other giants is

[8] See http://www.pha.jhu.edu/~stephan/h2ools2.html.

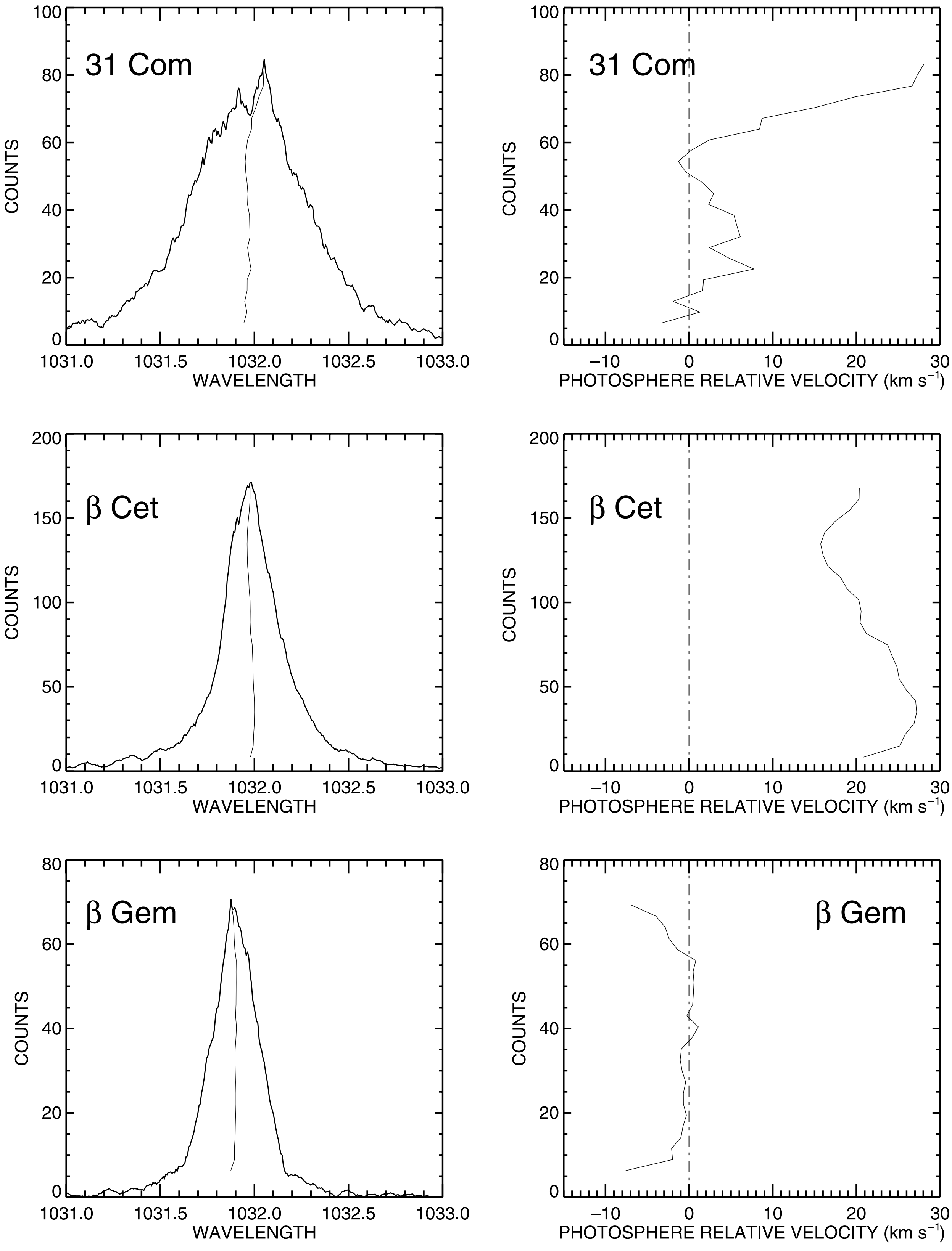

FIG. 13.—Bisectors of the O VI λ1032 emission in the giant stars. With the *FUSE* spectral resolution of 13–17 km s^{-1}, errors in centroiding are less than 2 km s^{-1}.

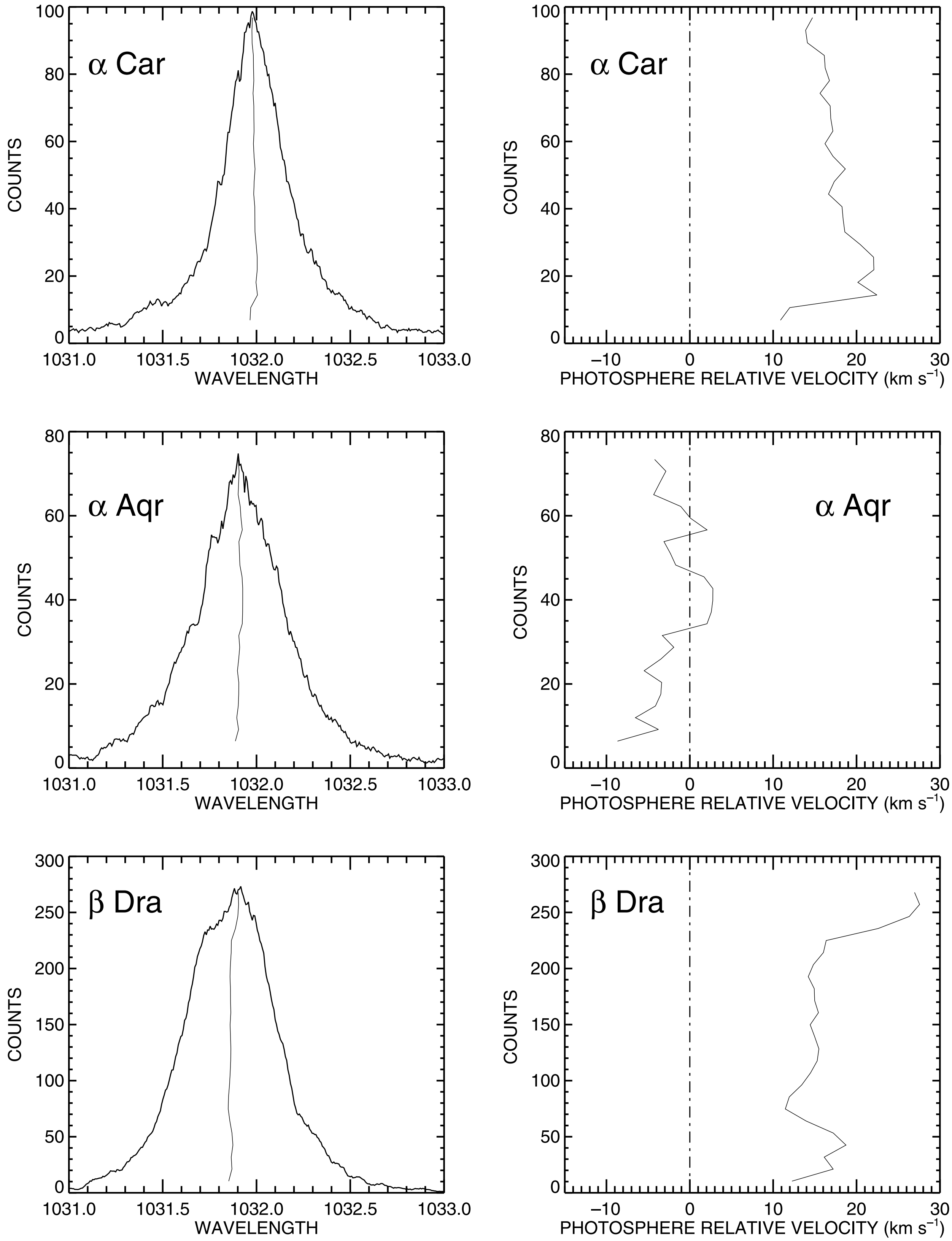

FIG. 14.—Bisectors of the O VI λ1032 emission in the supergiant stars.

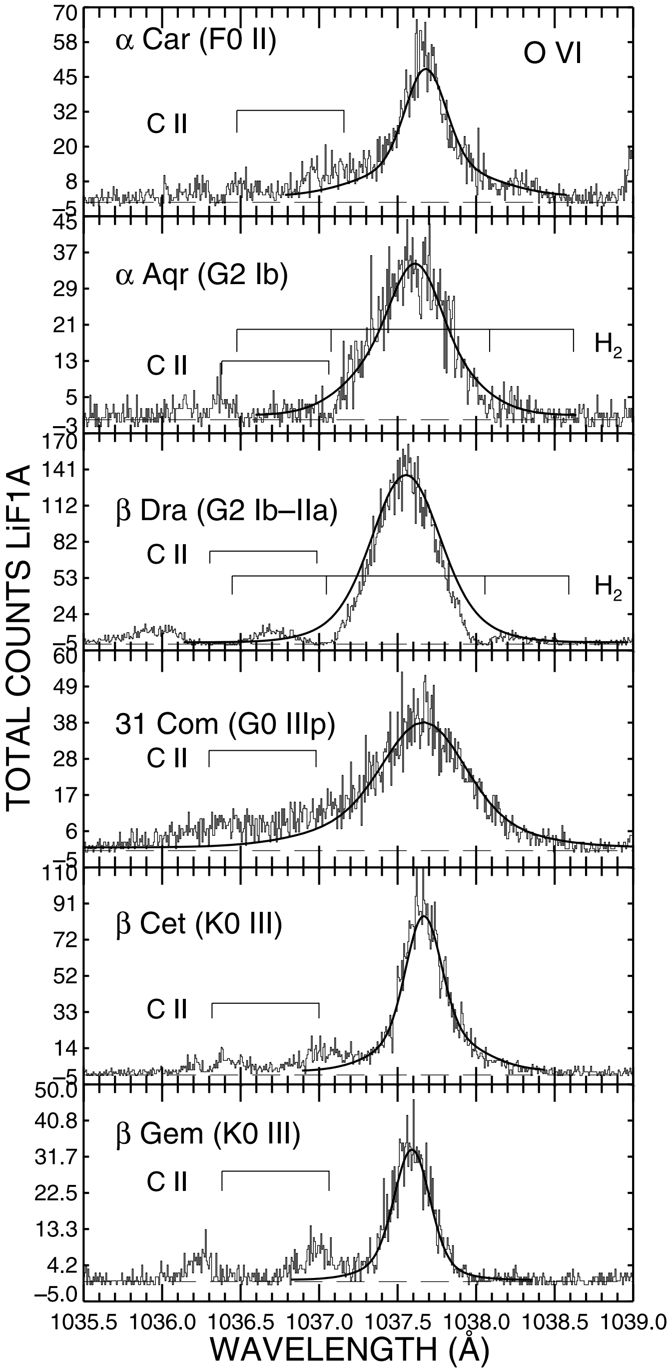

FIG. 15.—O VI λ1037 profile in target stars. A two-Gaussian fit to the corresponding O VI λ1032 line profile is overlaid, scaled by 0.5. Clearly β Dra and α Aqr give evidence for H_2 absorption indicated by absorption near the base of the profile. The C II emission doublet is present in many stars but can be affected by H_2 absorption.

consistent with formation by a magnetic dynamo process that becomes vigorous in fast rotators.

11.2. *Line Profiles*

Displaced Gaussian profiles have been observed in transition region emission lines in the Sun (Doschek et al. 1976; Peter & Judge 1999; Teriaca et al. 1999) and a wide variety of cool stars (Wood et al. 1997; Redfield et al. 2003; this paper). In the Sun, when observing a restricted atmospheric region ($\sim 1'' - 2''$ in size), Gaussians shifted to both shorter and longer wavelengths are found. The source of the redshifted emission has been attributed to many causes (unidirectional mass flows along magnetic loop structures, microflaring, heating effects, etc.), but no definitive identification of the causes of the redshifts has emerged (Peter 2004).

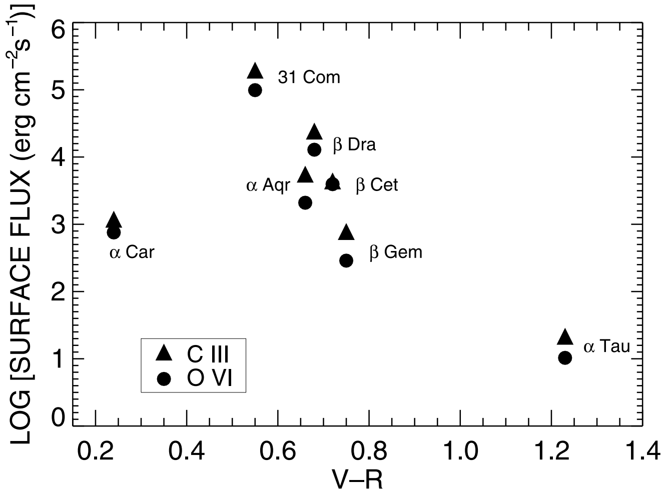

FIG. 16.—Emission-line flux in C III λ977 and O VI λ1032 at the stellar surface as a function of $(V-R)$. Uncertainties in the absolute flux are $\sim$10%, which are about the size of the plotted symbols.

The origin of the broad component in stellar line profiles of Si IV and C IV has been ascribed to microflare heating of the transition region (Wood et al. 1997) much as "explosive events" occur on the Sun. Additional evidence for this conjecture has been offered by the increase in the relative contribution of the broad component to the total flux accompanied by an increase in the C IV line flux and X-ray flux. This correlation suggested that enhanced heating contributes to the broad profile (Wood et al. 1997). The C III profiles studied here do not require two Gaussians (however, their distinctive asymmetries are discussed below). Moreover, the two components of O VI do not behave similarly to C IV in all stars (see Fig. 19) and show no systematic dependence on activity level. Thus, for luminous stars the behavior of a broad component does

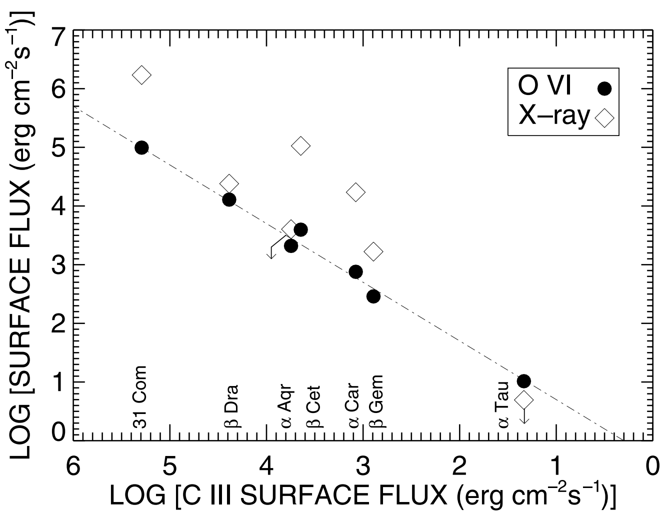

FIG. 17.—Tight correlation between C III λ977 and O VI λ1032 stellar surface flux (*filled circles*), which contrasts with the scattered relation between X-ray and C III flux (*open diamonds*). X-ray measures are taken from the *ROSAT* PSPC (0.1–2.4 keV) as reported by Ayres et al. (1995). X-ray values from Hünsch et al. (1996) for α Tau and Hünsch et al. (1998) for α Car are shown. X-ray fluxes for α Aqr and α Tau are upper limits. Errors on the measured fluxes of C III, O VI, and the X-ray flux are $\sim$10% or less.

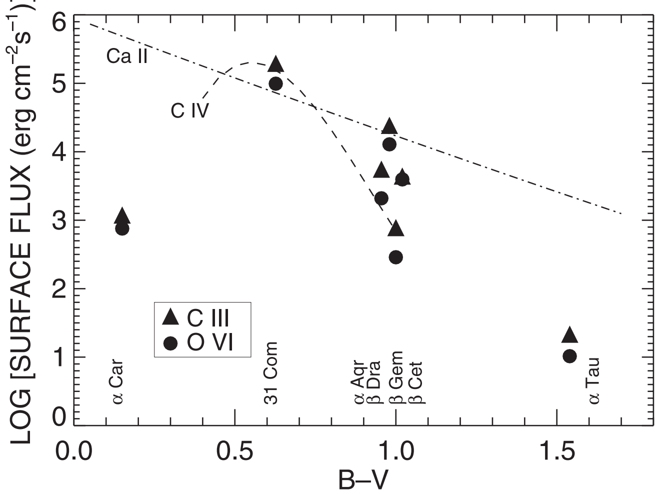

FIG. 18.—Surface fluxes in C III λ977 and O VI λ1032 as a function of $(B-V)$ for comparison to behavior of other emissions in giant stars. The net flux in Ca II (H and K) in open cluster giants (Dupree et al. 1999) and the C IV λ1550 flux (Ayres et al. 1995) are denoted by dot-dashed and dashed lines, respectively. Errors in measured fluxes are $\sim$10%, comparable to the size of the symbols.

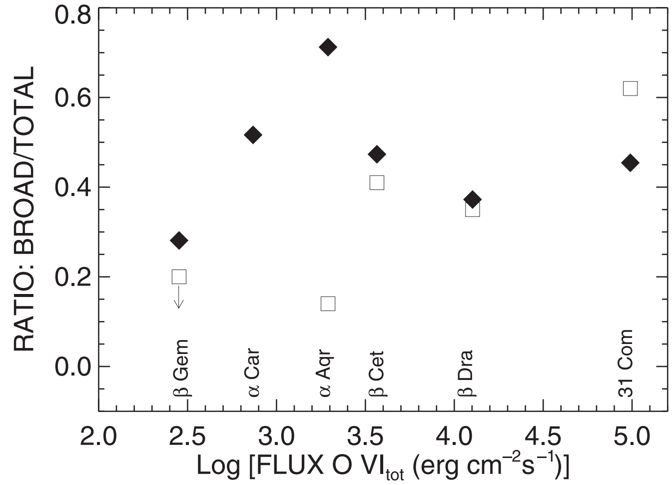

FIG. 19.—Ratio of the flux in the broad component of O VI to the total surface flux in the O VI λ1032 line (*filled diamonds*) as measured from Gaussian fits to the profiles. Results for some of the same stars from *HST* spectra of C IV λ1550 are shown (*open squares*; from Wood et al. 1997). The C IV ratio for α Aqr was measured from an *HST* GHRS archival spectrum. Formal errors in these ratios are on the order of $\pm$10% or less. Formal errors in the *FUSE* flux measurements are comparable to that value.

not appear similar to that identified in dwarf stars (Redfield et al. 2002). If such a relationship exists, it appears to be confined to the Si IV and C IV lines, as found by Wood et al. (1997), and does not extend to lower or higher temperatures.

Detailed studies of the C IV profiles in the Sun show that two-component fits are required only in the network regions, and not in the internetwork areas where one Gaussian suffices to match the profile. Moreover, emission from explosive events or transient brightenings is not related to the broad wings in the Sun (Peter & Brković 2003). A remaining possibility to interpret two-Gaussian fits appeals to the geometry of the transition region. Peter (2001) suggests that the broad wings on the solar disk originate from Alfvén wave–heated coronal funnels that accelerate the solar wind. Such broad wings are very apparent when viewing sections of the solar corona along a line of sight that traverses a coronal hole where a fast acceleration occurs. Outflow velocities >200 km s^{-1} significantly broaden the line profile (Miralles et al. 2001).

The luminous stars in this survey have extended atmospheres as a result in part of their low effective gravity, and it appears possible that much of the line broadening may be attributed to extension and expansion. This was first suggested by the observation of broad emission lines in hybrid stars as measured with *IUE* (Hartmann et al. 1981).

Analysis of the line profiles for dynamical signatures offers an explanation. The shapes of emission-line profiles can give clues to the atmospheric dynamics through the presence of line asymmetries. As Hummer & Rybicki (1968) first noted (and more recently Lobel & Dupree 2001), a differential expansion (or contraction) can cause red (or blue) asymmetries of the line profile. In complex multicomponent atmospheric modeling, when spatially averaging the contributions from many effectively optically thin components, each with potentially different velocity structures, the resulting line profile will be an appropriately weighted sum of the contribution function of each component.

The opacity at line center for a thermally broadened line is proportional to $A_Z \lambda f (M/T)^{1/2} N_e$, where A_Z is the elemental abundance with respect to hydrogen, λ is the wavelength of the line, f is the line oscillator strength, M is the mass of the atom, T is the temperature of formation, and N_e is the column density of electrons over the line-forming region. Although we do not yet have detailed models of the atmospheres of these stars, the atomic physics alone suggests that of the two major emission lines in the *FUSE* region, C III λ977 and O VI λ1032, the carbon line should have higher opacity (see also Harper 2001). This amounts to a factor of 2.5 for values of $A_Z \lambda f$ alone. It is expected that the electron column density will be higher for the C III line-forming region than for that of O VI since the emission measure distribution at C III temperatures exceeds that found at the higher temperatures of O VI (see Sanz-Forcada et al. 2003). Thus, we might expect that the λ977 profile would be more sensitive to dynamics.

Inspection of the C III line profiles (Fig. 9) shows a broad line, usually crossed by interstellar absorption, that is clearly asymmetric, displaying a lower flux at negative velocities than at positive velocities. This is obvious in the spectra of α Car, α Aqr, β Dra, and α Tau. Similar (although less pronounced) asymmetries are found in the C III profiles of β Cet and β Gem as illustrated by the single Gaussian fits to the emission. In both stars the line is asymmetric, suggestive of excess opacity in the line at negative velocities. The λ977 line from the fast rotating giant 31 Com possesses an FWHM $\sim$ 255 km s^{-1}. The $v \sin i$ of this giant (57 km s^{-1}; Strassmeier et al. 1994) is about half the observed line width, so clearly a line broadening mechanism in addition to rotation is present, perhaps extension of the atmosphere. The Gaussian fit to the long-wavelength wing of the profile suggests that additional opacity is present in 31 Com.

The O VI λ1032 profiles appear more symmetric than those of C III λ977. This might be expected because the opacity is less than in the carbon resonance line. It is not straightforward to predict the effects of opacity on the line profile. A higher optical depth is expected near the line center simply because the absorption profile reaches a maximum; thus, it is reasonable to expect the core to show signs of opacity.

All of the O VI lines (except for α Tau, which remains indeterminate because the count level is low) show an asymmetric profile. Two characteristics are apparent, irrespective of the absolute offset: three stars (β Dra, β Cet, and 31 Com) show a positive shift at the top of the profile (similar to that found in C III λ977) indicative of increased opacity on the short-wavelength side. This is the signature of absorption produced by outward-moving material in these stars.

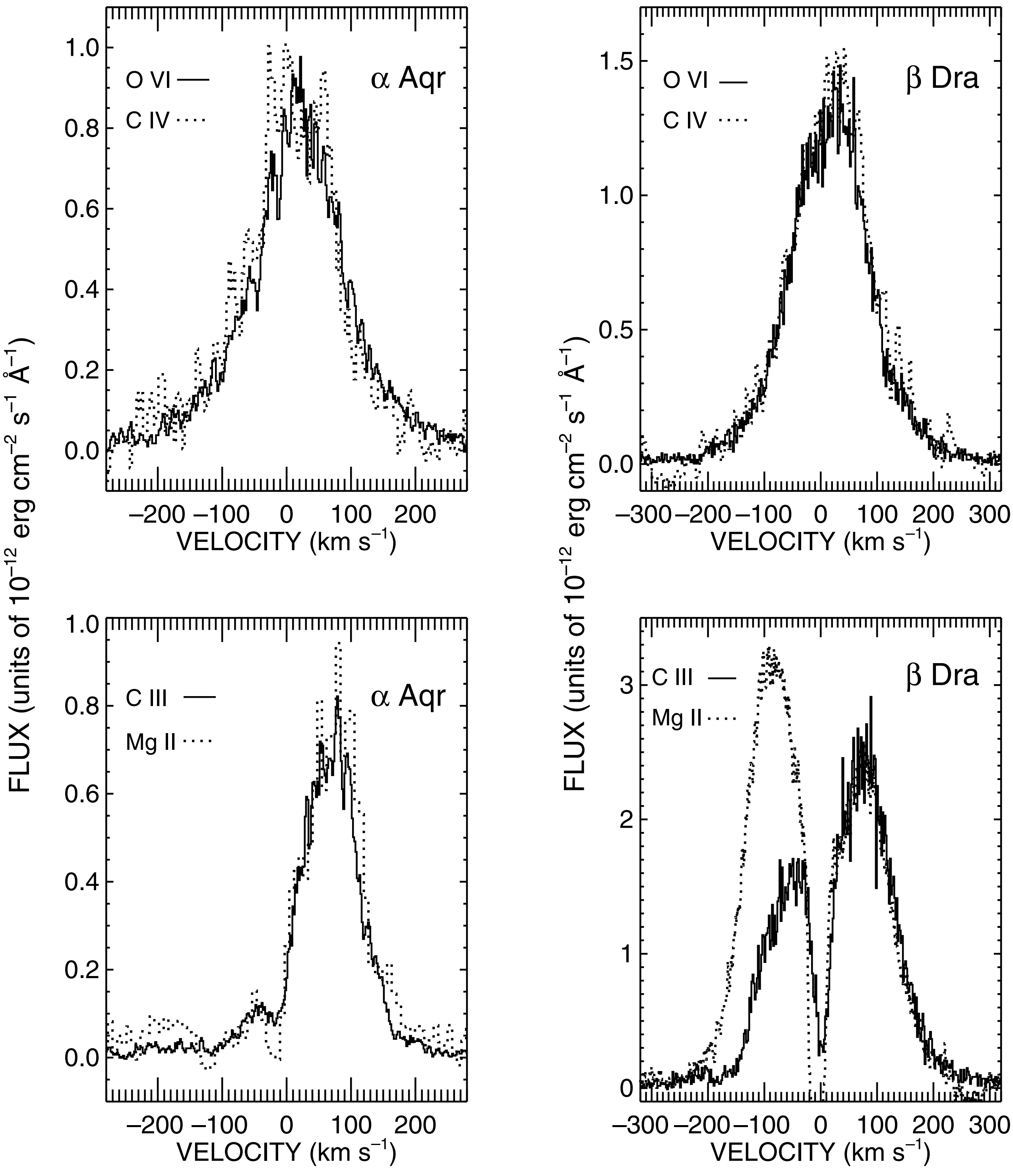

Fig. 20.—Comparison of C III and O VI from *FUSE* with other emission lines in the supergiants α Aqr and β Dra. For α Aqr, C IV $\lambda1548$ is taken from *HST* GHRS data set Z1FG010AM, and Mg II $\lambda2795$ from *IUE* LWR01390. For β Dra, C IV $\lambda1548$ is taken from *HST* GHRS data set Z2NW010CT, and Mg II $\lambda2795$ from *HST* GHRS data set Z0WZ0109T.

All bisectors exhibit a shift to negative velocities toward the base. Two interpretations for this behavior appear plausible. Either the opacity in a wind decreases as the expansion velocity approaches 100 km s^{-1}, or the extended stellar atmosphere blocks the extreme outward velocity of the atmosphere, creating a shift of the centroid to shorter wavelengths, or both.

Line widths are informative as well. Both α Car and α Aqr show exceptionally narrow core profiles, when compared to stars of similar luminosity, for instance, β Dra. As discussed further in the following section, the O VI width in most objects is comparable to that of the C IV line.

11.3. *Comparison with Ultraviolet Emission Lines*

The *FUSE* spectra of O VI sample the highest temperature transition region lines for which many line profiles are available; the C III profile is the most sensitive to optical depth. It is of interest to trace the atmospheric dynamics by comparing emission from C IV, Si III, and Mg II to the *FUSE* profiles. Profiles of

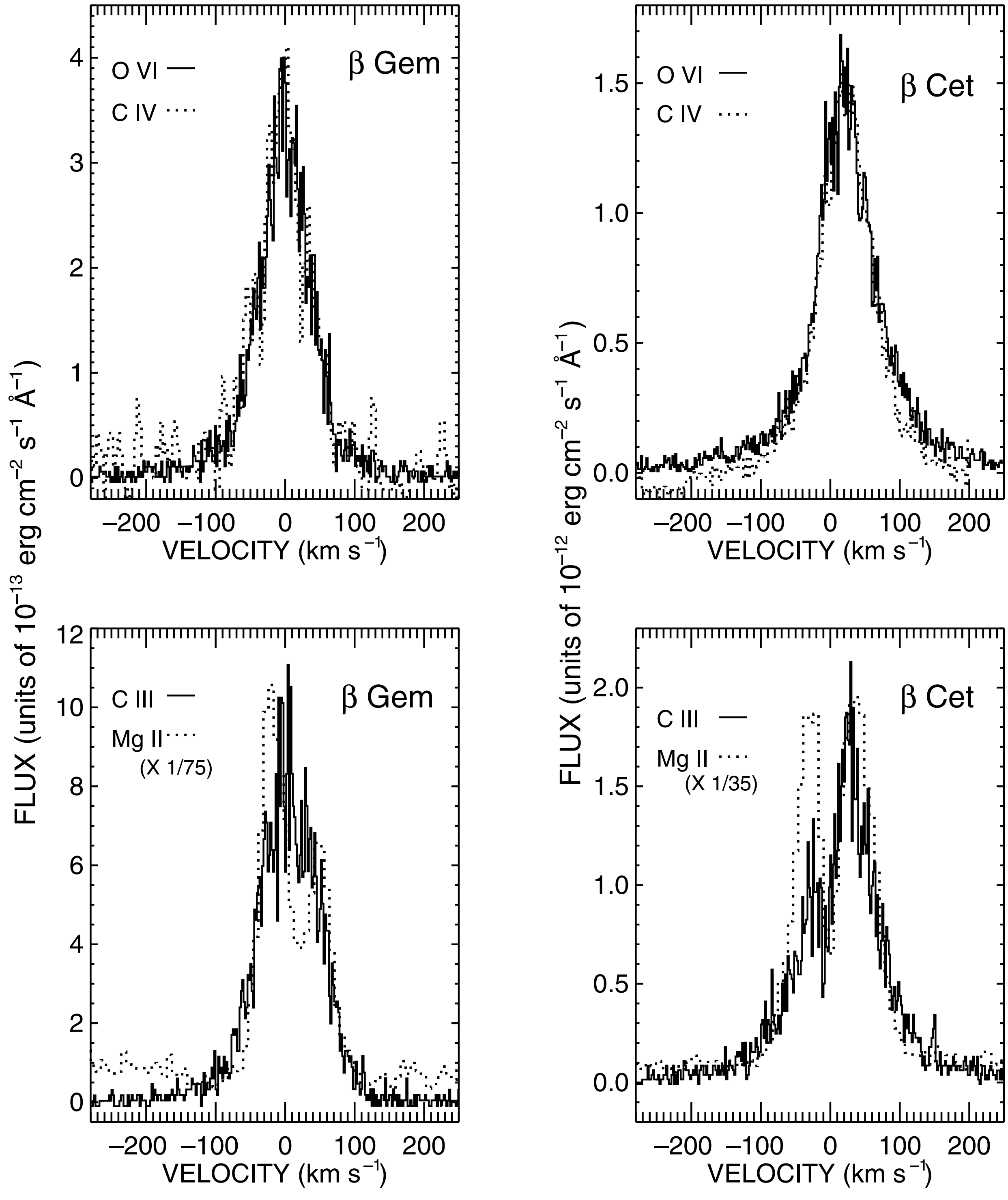

FIG. 21.—Comparison of C III and O VI from *FUSE* with other emission lines in the giants β Cet and β Gem. For β Cet, C IV λ1548 is taken from *HST* STIS data set O5B701020, and Mg II λ2795 from *IUE* LWP 08615. For β Gem, C IV λ1548 is taken from *HST* GHRS data set Z2UZ010FT, and Mg II λ2795 from *IUE* LWP 27482.

the supergiants α Aqr and β Dra are shown in Figure 20. Whereas α Aqr shows good agreement between the asymmetry of the C III λ977 line and Mg II, indicating outflow and absorption at velocities up to -100 km s^{-1} or more, β Dra spectra indicate that the outflow does not occur at the cooler levels of Mg II, but at the higher temperatures represented by C III. Variable opacity has been noted on the short-wavelength side of the C IV line in β Dra (Wood et al. 1997), which provides evidence for a wind at transition region temperatures. It is thought that β Dra may be in a prehybrid phase. Star α Aqr is a well-known "hybrid" star where the wind is well developed and detectable throughout the atmosphere; supersonic acceleration has even been identified in the chromosphere (Dupree et al. 1992). The C IV and O VI lines are similar in width in both supergiants, and the asymmetry of the peak of the core emission persists in C III, C IV, and O VI in β Dra. Comparison of profiles for the giant stars is shown in Figures 21, 22, and 23. With the exception of β Gem, the other giant stars, β Cet, 31 Com, and α Tau, show opacity in the C III line that is frequently matched

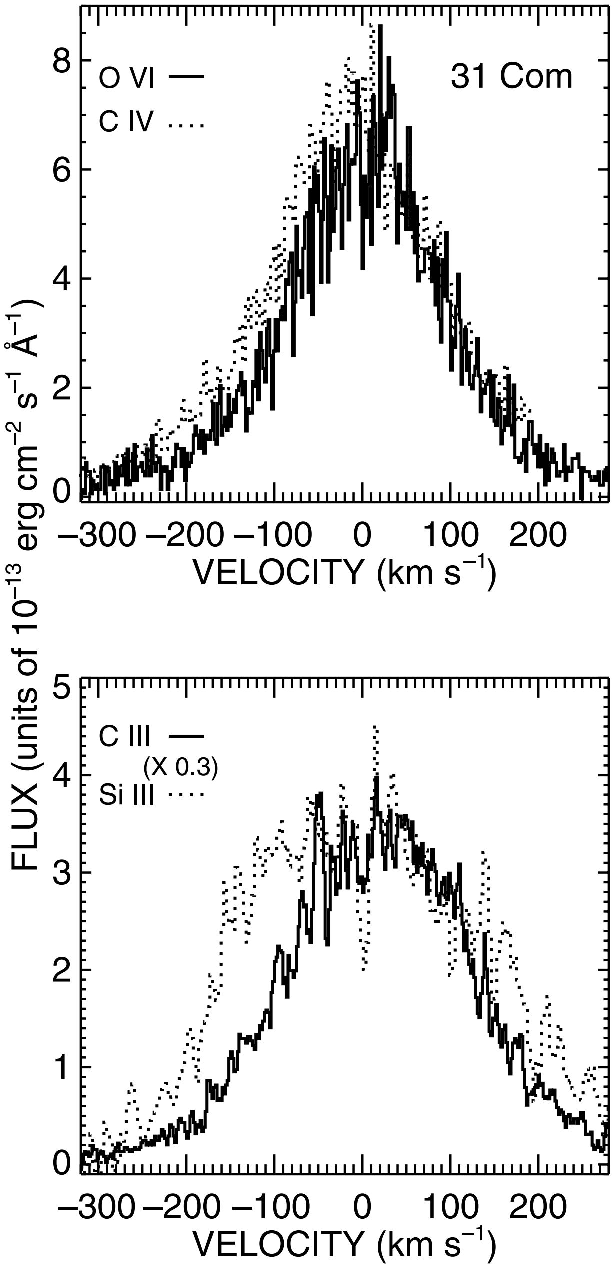

FIG. 22.—Comparison of C III and O VI from *FUSE* with other emission lines in 31 Com. The C IV λ1548 profile is taken from *HST* STIS data set O6AQ01010, and Si III λ1206 from *HST* STIS data set O6AQ01020.

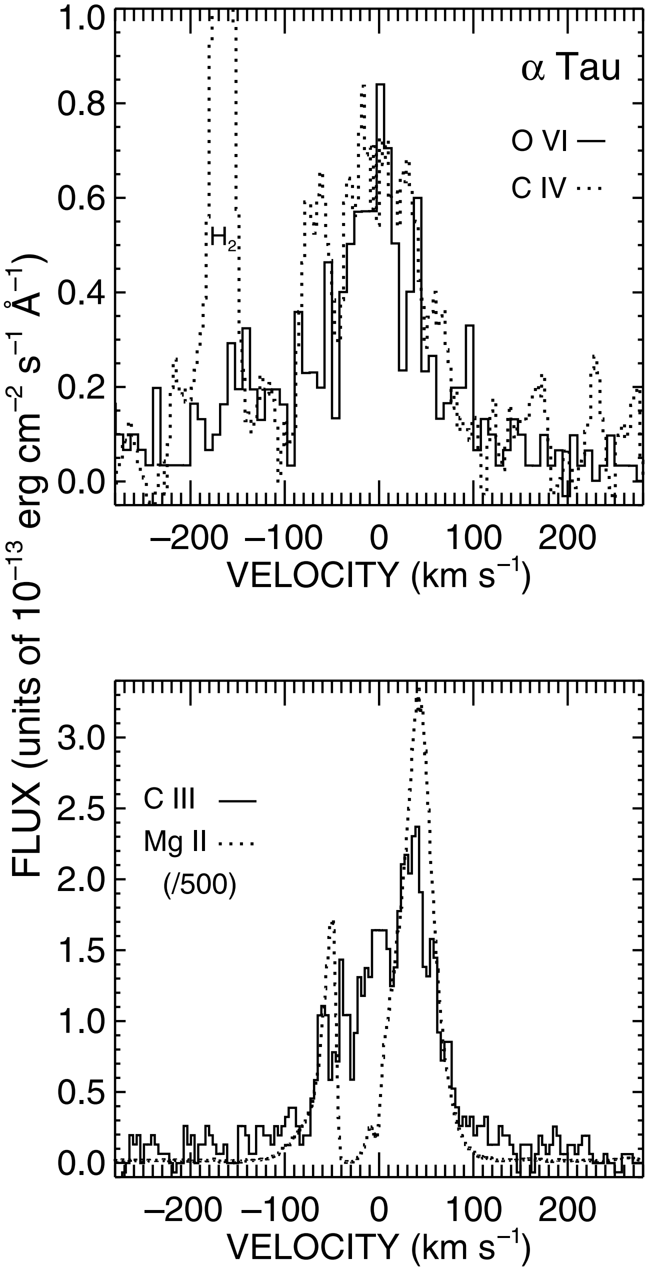

FIG. 23.—Comparison of C III and O VI with other emission lines in α Tau. The C IV profile is from *HST* STIS data set O6JE01020, and the Mg II profile from *HST* GHRS data set Z3FX020BT.

with a similar asymmetry in Mg II or Si III. Star β Gem is more like β Dra with chromospheric infall indicated by the Mg II line shape. Since these spectra come from diverse sources, including *IUE*, *HST* GHRS, and *HST* STIS, they have been scaled in flux and at times shifted to compare profile shapes.

It is puzzling that the O VI λ1032 line widths are generally comparable to the C IV λ1548 transitions and both are broadened in excess of pure thermal broadening. In the solar network, O VI is observed to be broader than the C IV line (Peter 2001), by a factor of 1.2–1.4; the nonthermal contributions are also higher in the Sun for O VI than C IV. The observed O VI line width of the core exceeds the thermal width expected at 3×10^5 K by factors of 3 or more. Clearly atmospheric extension, turbulence, and/or opacity can affect these line profiles.

Could the character of the atmosphere change dramatically at the $\sim$200,000 K level from a relatively homogeneous outflow (indicated by the broad asymmetric C III profiles) to an atmosphere covered by magnetic loop structures signaled by the narrow redshifted C IV and O VI lines? We have no estimate of the densities in the regions forming C IV and O VI, so it is unclear whether small scales are indicated (as they are for dense coronal material). Lower turbulent velocities and/or less geometrical broadening might be plausible in such structures although they are not required for confinement because thermal motion of material at the temperature of 3×10^5 K (18 km s^{-1}) is an order of magnitude less than the escape velocity from giant stars (200 km s^{-1}). As noted earlier, identifying the redshifted emission profiles of O VI with physical atmospheric downflows requires synchronous motion among all putative loops covering the giant or supergiant stars, or a judicious combination of many regions with individual dynamics that systematically produce a redshifted line. We cannot firmly eliminate some distribution of emitting regions over the stellar surface that produces a redshifted asymmetric emission-line profile. However, the identical nature of the C IV and O VI line profiles (measured at different times) suggests that they are not dominated by transient active regions or varying downflow emission profiles.

Could wind opacity effects narrow the lines, causing O VI and C IV to be less broad than C III? Without a detailed model, it is difficult to assess the relative opacities in the C IV and O VI transitions. A comparison of the quantity $f\lambda A_{el}$ using solar abundances suggests that C IV opacity values exceed O VI by 20%. However, luminous stars are evolved, and it is well known that the CN cycle depletes carbon (enhancing nitrogen). Although classical studies suggest that both carbon and oxygen are underabundant with respect to solar values (Luck & Lambert 1985), there is currently controversy about the difficult-to-measure oxygen abundances (Fulbright & Johnson 2003). The line shapes strongly suggest that opacity plays a role; clearly modeling is needed.

11.4. *Relationship to Coronal Lines*

Two of our targets show coronal line emission in the *FUSE* region, and others are X-ray sources. The *FUSE* spectra suggest that the coronal lines occur near photospheric radial velocities and so do not participate in any outflow (see also Redfield et al. 2003). This is consistent with the fact that plasma at coronal temperatures (here $\sim 6 \times 10^8$ K) must be confined by magnetic fields in these stars. Such confinement was postulated when Fe XVIII and Fe XIX species were first identified as a stable feature in the *EUVE* spectra of the giant stars of Capella (Dupree et al. 1993; Young et al. 2001). Confinement is consistent with the small sizes inferred from the high densities of the coronal regions at these temperatures (Sanz-Forcada et al. 2003). These *FUSE* results suggest an inhomogeneous atmosphere in which small magnetic features at high temperature are anchored in the presence of a warm expanding atmosphere.

12. CONCLUSIONS

We list our conclusions as follows:

1. The presence of warm 3×10^5 K plasma, indicated by O VI emission, appears ubiquitous and extends across the H-R diagram. The K5 giant, α Tau, is the coolest giant to exhibit O VI known to date.
2. The atmosphere of the M supergiant α Ori does not exhibit any C III or O VI emission, suggesting maximum temperatures less than 80,000 K if collisionally dominated.
3. The decay of stellar surface emission with decreasing temperature for both C III and O VI suggests that similar magnetic processes are responsible for these emissions.
4. An outward acceleration of 80,000 K material, clearly indicated by the C III emission profiles, occurs in all these stars from F0 II through K5 III (α Tau), clearly demonstrating the presence of a warm wind.
5. The O VI λ1032 emission gives some evidence also of wind opacity in most stars, suggesting that warmer winds of 300,000 K may be present.
6. Semiempirical modeling of atmospheres and winds and of the emergent chromospheric and transition region line profiles is needed for luminous cool stars.

This work is based on data obtained for the Guaranteed Time Team by the NASA-CNES-CSA *FUSE* mission operated by the Johns Hopkins University. Financial support to US participants has been provided by NASA contract NAS5-32985.

REFERENCES

Achour, H., Brekke, P., Kjeldseth-Moe, O., & Maltby, P. 1995, ApJ, 453, 945
Ake, T., B., Dupree, A. K., Young, P. R., Linsky, J. L., Malina, R. F., Griffiths, N. W., Siegmund, O. H. W., & Woodgate, B. E. 2000, ApJ, 538, L87
Ayres, T. R., Brown, A., Harper, G. M., Osten, R. A., Linsky, J. L., Wood, B. E., & Redfield, S. 2003, ApJ, 583, 963
Ayres, T. R., Brown, A., Osten, R. A., Huenemoerder, D. P., Drake, J. J., Brickhouse, N. S., & Linsky, J. L. 2001a, ApJ, 549, 554
Ayres, T. R., Osten, R. A., & Brown, A. 1999, ApJ, 526, 445
———. 2001b, ApJ, 562, L83
Ayres, T. R., Simon, T., Stern, R. A., Drake, S. A., Wood, B. E., & Brown, A. 1998, ApJ, 496, 428
Ayres, T. R., et al. 1995, ApJS, 96, 223
Baliunas, S. L., Guinan, E. F., & Dupree, A. K. 1984, ApJ, 282, 733
Barnes, T. G., Evans, D. S., & Moffett, T. J. 1978, MNRAS, 183, 285
Beavers, W. I., & Eitter, J. J. 1986, ApJS, 62, 147
Bookbinder, J., Walter, F., & Brown, A. 1992, in ASP Conf. Ser. 26, Seventh Cambridge Workshop on Cool Stars, Stellar Systems, and the Sun, ed. M. Giampapa & J. Bookbinder (San Francisco: ASP), 27
Brown, A., Deeney, B. D., Ayres, T. R., Veale, A., & Bennett, P. D. 1996, ApJS, 107, 263
Buchholz, B., Ulmschneider, P., & Cuntz, M. 1998, ApJ, 494, 700
Carpenter, K. C., Robinson, R. D., Harper, G. M., Bennett, R. D., Brown, A., & Mullan, D. J. 1999, ApJ, 521, 382
Cash, W. 1979, ApJ, 228, 939
Curdt, W., Brekke, P., Feldman, U., Wilhelm, K., Dwivedi, B. N., Schühle, U., & Lemaire, P. 2001, A&A, 375, 591
Del Zanna, G., Landini, M., & Mason, H. 2002, A&A, 385, 968
de Medeiros, J. R., & Mayor, M. 1999, A&AS, 139, 433
Dere, K. P., Landi, E., Young, P. R., & Del Zanna, G. 2001, ApJS, 134, 331
Doschek, G. A., Bohlin, J. D., & Feldman, U. 1976, ApJ, 205, L177
Doyle, J. G., & McWhirter, R. W. P. 1980, MNRAS, 193, 947
Drake, S. A., Brown, A., & Linsky, J. L. 1984, ApJ, 284, 774
Dring, A. R., Linsky, J., Murthy, J., Henry, R. C., Moos, W., Vidal-Madjar, A., Audouze, J., & Landsman, W. 1997, ApJ, 488, 760
Dupree, A. K., & Brickhouse, N. S. 1995, in IAU Symp. 176, Poster Proceedings, ed. K. G. Strassmeier (Vienna: Institut für Astron. Univ. Vienna), 184
———. 1998, ApJ, 500, L33
Dupree, A. K., Brickhouse, N. S., Doschek, G. A., Green, J. C., & Raymond, J. C. 1993, ApJ, 418, L41
Dupree, A. K., Foukal, P. V., & Jordan, C. 1976, ApJ, 209, 621
Dupree, A. K., & Reimers, D. 1989, in Exploring the Universe with the *IUE* Satellite, ed. Y. Kondo (Boston: Kluwer), 321
Dupree, A. K., Whitney, B. A., & Avrett, E. H. 1992, in ASP Conf. Ser. 26, Seventh Cambridge Workshop on Cool Stars, Stellar Systems, and the Sun, ed. M. Giampapa & J. Bookbinder (San Francisco: ASP), 525
Dupree, A. K., Whitney, B. A., & Pasquini, L. 1999, ApJ, 520, 751
Fekel, F. 1997, PASP, 109, 514
Fulbright, J. P., & Johnson, J. A. 2003, ApJ, 595, 1154
Gómez de Castro, A. I. 2002, MNRAS, 332, 409
Harper, G. M. 2001, in ASP Conf. Ser. 223, Eleventh Cambridge Workshop on Cool Stars, Stellar Systems, and the Sun, ed. R. J. García López, R. Rebolo, & M. R. Zapatero Osorio (San Francisco: ASP), 368
Harper, G. M., Wilkinson, E., Brown, A., Jordan, C., & Linsky, J. L. 2001, ApJ, 551, 486
Hartman, H., & Johansson, S. 2000, A&A, 359, 627
Hartmann, L., Dupree, A. K., & Raymond, J. C. 1980, ApJ, 236, L143
———. 1981, ApJ, 246, 193
Hummer, D., G., & Rybicki, G. B. 1968, ApJ, 153, L107
Hünsch, M., Schmitt, J. H. M. M., Schröder, K.-P., & Reimers, D. 1996, A&A, 310, 801
Hünsch, M., Schmitt, J. H. M. M., & Voges, W. 1998, A&AS, 127, 251
Hünsch, M., & Schröder, K.-P. 1996, A&A, 309, L51
Johnson, H. L., Iriarte, B., Mitchell, R. I., & Wisniewskj, W. J. 1966, Comm. Lunar Planet. Lab., 4, 99
Jordan, C., & Linsky, J. L. 1989, in Exploring the Universe with the IUE Satellite, ed. Y. Kondo (Boston: Kluwer), 259
Jordan, C., McMurry, A. D., Sim, S. A., & Arulvel, M. 2001, MNRAS, 322, L5
Kaufman, V., & Martin, W. C. 1989, J. Opt. Soc. Am. B, 6, 1769

Lehner, N., Jenkins, E. B., Gry, C., Moos, H. W., Chayer, P., & Lacour, S. 2003, ApJ, 595, 858
Lemaire, P., Emerich, C., Vial, J.-C., Curdt, W., Schuhle, U., & Wilhelm, K. 2002, in Proc. SOHO-11: From Solar Minimum to Maximum (ESA SP-508; Noordwijk: ESA), 219
Linsky, J. L., & Wood, B. E. 1994, ApJ, 430, 342
Lobel, A., & Dupree, A. K. 2001, ApJ, 558, 815
Luck, R. E., & Lambert, D. L. 1985, ApJ, 298, 782
Marilli, E., Catalano, S., Freire Ferrero, R., Gouttebroze, P., Bruhweiler, F., & Talavara, A. 1997, A&A, 317, 521
Mazzotta, P., Mazzitelli, G., Colafrancesco, S., & Vittorio, N. 1998, A&AS, 133, 403
McCandliss, S. R. 2003, PASP, 115, 651
McMurry, A. D., & Jordan, C. 2000, MNRAS, 313, 423
Miralles, M. P., Cranmer, S. R., & Kohl, J. L. 2001, ApJ, 560, L193
Moos, W. H., et al. 2000, ApJ, 538, L1
Nousek, J. A., & Shue, D. R. 1989, ApJ, 342, 1207
Perryman, M. A. C., et al. 1997, A&A, 323, L49
Peter, H. 2001, A&A, 374, 1108
———. 2004, IAU Symp. 219, Stars as Suns: Activity Evolution, and Planets, ed. A. K. Dupree & A. O. Benz (San Francisco: ASP), 575
Peter, H., & Brković, A. 2003, A&A, 403, 287
Peter, H., & Judge, P. G. 1999, ApJ, 522, 1148
Piskunov, N., Wood, B. E., Linsky, J. L., Dempsey, R. C., & Ayres, T. R. 1997, ApJ, 474, 315
Rao, L. M, Baliunas, S. L., Robinson, C. R., Frazer, J., Woodard, L., & Donahue, R. A. 1993, in ASP Conf. Ser. 45, Luminous High Latitude Stars, ed. D. D. Sasselov (San Francisco: ASP), 300
Redfield, S., Ayres, T. R., Linsky, J. L., Ake, T. B., Dupree, A. K., Robinson, R. D., & Young, P. R. 2003, ApJ, 585, 993
Redfield, S., & Linsky, J. 2004, ApJ, 602, 776
Redfield, S., Linsky, J. L., Ake, T. B., Ayres, T. R., Dupree, A. K., Robinson, R. D., Wood, B. E., & Young, P. R. 2002, ApJ, 581, 626
Reimers, D. 1977, A&A, 57, 395
Reimers, D., Hünsch, M., Schmitt, J. H. M. M., & Toussaint, F. 1996, A&A, 310, 813
Robinson, R. D., Carpenter, K. G., & Brown, A. 1998, ApJ, 503, 396
Robinson, R. D., Linsky, J. L., Woodgate, B. E., & Timothy, J. G. 2001, ApJ, 554, 368
Robinson, R. D., et al. 1992, in ASP Conf. Ser. 26, Cool Stars, Stellar Systems, and the Sun, ed. M. S. Giampapa & J. A. Bookbinder (San Francisco: ASP), 31
Rutten, R. G. M., & Pylyser, E. 1988, A&A, 191, 227
Sahnow, D. J., et al. 2000, ApJ, 538, L7
Sanz-Forcada, J., Brickhouse, N. S., & Dupree, A. K. 2002, ApJ, 570, 799
———. 2003, ApJS, 145, 147
Schaller, G., Schaerer, D., Meynet, G., & Maeder, A. 1992, A&AS, 96, 269
Smith, R. K., Brickhouse, N. S., Liedahl, D. A., & Raymond, J. C. 2001, ApJ, 556, L91
Strassmeier, K. G., Washüttl, A., & Rice, J. B. 1994, Inf. Bull. Variable Stars, 3994, 1
Teriaca, L., Banerjee, D., & Doyle, J. G. 1999, A&A, 349, 636
Wilson, R. E. 1953, General Catalogue of Stellar Radial Velocities (Washington: Carnegie Institution)
Withbroe, G., & Noyes, R. W. 1977, ARA&A, 15, 363
Wood, B. E., Linsky, J. L., & Ayres, T. R. 1997, ApJ, 478, 745
Young, P. R., Del Zanna, G., Landi, E., Dere, K. P., Mason, H. W., & Landini, M. 2003, ApJS, 144, 135
Young, P. R., Dupree, A. K., Wood, B. E., Redfield, S., Linsky, J. L., Ake, T. B., & Moos, H. W. 2001, ApJ, 555, L121